Titre: Title:	Étude de la perforation radio fréquence du tissu cardiaque
Auteur: Author:	Nelli Shimko
Date:	1999
Type:	Mémoire ou thèse / Dissertation or Thesis
Référence: Citation:	Shimko, N. (1999). Étude de la perforation radio fréquence du tissu cardiaque [Master's thesis, École Polytechnique de Montréal]. PolyPublie. https://publications.polymtl.ca/8677/

UNIVERSITÉ DE MONTRÉAL

ÉTUDE DE LA PERFORATION RADIO FRÉQUENCE DU TISSU CARDIAQUE

NELLI SHIMKO
INSTITUT DE GÉNIE BIOMÉDICAL
ÉCOLE POLYTECHNIQUE DE MONTRÉAL

MÉMOIRE PRÉSENTÉ EN VUE DE L'OBTENTION
DU DIPLÔME DE MAÎTRISE ÈS SCIENCES APPLIQUÉES
(GÉNIE BIOMÉDICAL)

SEPTEMBRE 1999

UNIVERSITÉ DE MONTRÉAL
ÉCOLE POLYTECHNIQUE DE MONTRÉAL

Ce mémoire intitulé:

ÉTUDE DE LA PERFORATION RADIO FRÉQUENCE DU TISSU CARDIAQUE

présenté par : SHIMKO Nelli
en vue de l'obtention du diplôme de: Maîtrise ès Sciences Appliquées
a été dûment accepté par le jury d'examen constitué de :

M. LEON L. Joshua, Ph.D., président
M. SAVARD Pierre, Ph.D., membre et directeur de recherche
M. GUARDO Robert, Ph.D., membre

ACKNOWLEDGEMENTS

I express my gratitude to my supervisor and mentor Pierre Savard. He, more than anybody else, has contributed toward success of my studies and this project. His talents, professional and pedagogical, have served me as an example.

I am grateful to professor Robert Guardo, to Denis Guerette and to Pierre Le Gyader for their technical support in the experimental part of my project.

I am equally grateful toward members and students of the group of modeling in biomedicine for their expression of friendship and their technical assistance.

In conclusion, I am thankful for the financial support from the Baylis company and National Science Foundation of Canada.

RÉSUMÉ

Le courant radio fréquence (RF) injecté par un mince cathéter peut être utilisé pour perforer la valve pulmonaire ou le septum auriculaire pour le traitement de l'atrésie pulmonaire avec septum ventriculaire intact chez les nouveau-nés.

L'atrésie pulmonaire avec septum ventriculaire intact est une malformation du cœur humain. Cette anomalie est caractérisée par l'obstruction complète à l'écoulement sanguin du ventricule droit vers le tronc pulmonaire à cause de l'occlusion de la valve pulmonaire. Le sang veineux arrive à la partie gauche du cœur par le foramen ovale en se mêlant avec le sang oxygéné de l'oreillette gauche. Ce mélange entre dans le ventricule gauche et ensuite dans l'aorte. Le sang aortique trouve son chemin vers la circulation pulmonaire par le ductus (canal artériel). L'écoulement pulmonaire est habituellement très déficient. La cyanose survient à la naissance. Dès que le ductus se ferme, l'écoulement sanguin dans le lit pulmonaire s'arrête, entraînant la mort.

Le traitement chirurgical des nouveau-nés avec atrésie pulmonaire et septum ventriculaire intact cause une morbidité et une mortalité élevées. Récemment, un petit cathéter RF a permis la perforation et la dilatation de la valve pulmonaire atrésiée par un ballon. Malgré ce succès chirurgical, beaucoup d'aspects de la perforation RF restent encore inconnus.

Afin d'étudier les concepts importants de la perforation RF et de déterminer les paramètres optimaux du cathéter et du courant, un modèle numérique a été développé et des expériences ont été effectuées. Ce modèle axisymétrique se compose d'un domaine cylindrique avec une couche du tissu entre deux couches de sang. Une différence de potentiel est appliquée entre le bout du cathéter et une électrode indifférente de grande dimension. Dès que la température produite par le courant circulant dans le tissu dépasse

100°C dans tous les éléments du modèle qui se trouvent directement en face de cathéter, ceux-ci sont considères instantanément vaporisés, et le cathéter avance au-delà de ces éléments, simulant ainsi la perforation. La méthode des différences finies est utilisée pour les calculs de potentiel et de température, puisqu'elle permet de conserver le même maillage au fur et à mesure de l'avance du cathéter.

Dès expériences sur du tissu cardiaque canin (paroi auriculaire et feuillet valvulaire) furent aussi effectués pour valider le modèle. Pendant l'application de basse puissance, la température calculée par le modèle coïncide avec la température mesurée. La perforation a eu lieu lorsque le voltage appliqué a dépassé 70 – 80 V dans le myocarde, ce qui coïncide aussi avec les résultats simulés. L'étendue latérale du tissu endommagé était plus petite avec un voltage élevé à cause de la perforation rapide. Les électrodes courtes et de petit diamètre ont produit les perforations les plus rapides.

En conclusion, la simulation numérique de la perforation RF a permis de déterminer les paramètres optimaux du cathéter et du courant afin de rendre la perforation RF prédictible et curative.

ABSTRACT

Radio frequency (RF) current delivered through the tip of a thin catheter can be used to perforate the pulmonary valve or atrial septum for the treatment of pulmonary atresia with intact ventricular septum in newborns.

Pulmonary atresia is a malformation of the human heart. It is characterized by the complete obstruction to forward blood flow from the right ventricle into the pulmonary trunk because of a pulmonary valve imperforation or closure. Venous blood reaches the left side of the heart via the foramen ovale, mixing with oxygenated blood in the left atrium. This mixture flows into the left ventricle and aorta. Aortic blood finds its way into the pulmonary circulation via the normally formed ductus arteriosus. The pulmonary flow is usually deficient. Cyanosis begins at or immediately after birth. When the ductus closes, effective blood flow into the pulmonary bed stops and death follows shortly.

Surgical treatment of neonates with pulmonary atresia and intact ventricular septum is associated with high morbidity and mortality. Recently, RF catheterization was used for the perforation and subsequent balloon dilatation of the atretic pulmonary valve. Despite some success, many aspects of RF perforation of cardiac tissues remain unclear.

In an attempt to gain more insight into the process of RF perforation for the purpose of identifying the design features of the catheter and the RF current delivery, a numerical model was developed and experiments were performed. This axisymmetrical model consists of a cylindrical domain with a tissue layer between two blood layers. A potential difference is applied between the catheter tip and a large distant electrode. When the temperature produced by the RF current flowing inside the tissue exceeds 100°C in all the elements that are directly in front of the catheter, these elements are considered to be instantly vaporized and the catheter advances over these elements, thus

simulating perforation. The finite difference method was used for the potential and temperature computations because it allowed keeping the same mesh during the catheter advancement through the tissue.

Experiments were also conducted in isolated canine cardiac tissue (atrial wall and valve leaflets). The computed temperature time course coincided with measured temperature at small power setting. Simulated perforation occurred when the applied voltage exceeded 70-80 V in the myocardium, which also coincided with experimental observations. The lateral extent of tissue damage was smaller with higher voltage because of more rapid perforation. Shorter electrodes with smaller diameters produced more rapid perforation.

In conclusion, the mathematical simulation of the RF perforation allowed the determination of optimal design parameters of the catheter and optimizing the RF current delivery in order to make RF perforation predictable and curative.

CONDENSÉ EN FRANÇAIS

L'étude a pour but de définir les paramètres physiques impliqués dans la perforation radio fréquence (RF) de la valve pulmonaire pour traiter l'atrésie pulmonaire avec septum ventriculaire intact chez les nouveau-nés.

L'ATRÉSIE PULMONAIRE ET SES TRAITEMENTS

L'atrésie pulmonaire est caractérisée par l'obstruction à l'écoulement sanguin entre le ventricule droit et le tronc pulmonaire. La valve pulmonaire est soit non-perforée, soit obstruée par du tissu musculaire ou fibromusculaire. Le sang arrivant dans la partie droite du cœur passe de l'oreillette droite à l'oreillette gauche par le foramen ovale (l'ouverture au niveau de septum auriculaire). Le sang est ensuite expulsé dans l'aorte pendant la contraction du ventricule gauche. Par rapport à la circulation normale, la circulation pulmonaire est très réduite et s'approvisionne grâce à une jonction entre l'aorte et l'artère pulmonaire appelée le canal artériel (ductus arteriosus) qui normalement se ferme quelques semaines après la naissance.

Il y a deux types d'atrésie pulmonaire qui dépendent de la taille du ventricule droit et de la compétence de la valve tricuspide. Le premier type, plus fréquent, est caractérisé par un ventricule droit diminué avec des parois épaisses et une valve tricuspide compétente. Les sinusoïdes, ou vaisseaux sanguins, traversant la paroi du ventricule droit sont fermées au niveau de l'épicarde, ou ils communiquent avec une artère coronaire. Les sinusoïdes fermées entraînent la rupture du myocarde à cause de la pression diastolique excessive, tandis que les sinusoïdes liées à l'artère coronaire entraînent un infarctus du myocarde. Le deuxième type, moins fréquent, est caractérisé par un ventricule normal et une valve tricuspide non compétente.

La survie dépend de la compétence de la communication entre la voie aortique et le tronc pulmonaire, de la taille de la communication entre les oreillettes et des autres caractéristiques anatomiques de cette pathologie (les sinusoïdes, l'hypotrophie ventriculaire). Selon les données statistiques, la majorité des enfants meurent pendant les trois premiers mois de la vie, aussitôt que le ductus arteriosus devient incompétent, et peu d'enfants survivent au-delà d'une année.

Le traitement de l'atrésie pulmonaire par chirurgie n'est pas satisfaisant à cause de la taille minuscule du cœur des nouveau-nés. Ce traitement chirurgical s'accompagne malheureusement de taux de mortalité et morbidité élevé. Récemment, une nouvelle technique minimalement invasive, la perforation radio fréquence par un cathéter mince, a été proposée afin de perforer la valve pulmonaire. Toutefois, les données techniques présentées par les auteurs sont incomplètes et très variables. Par exemple, deux types de courant, continu et pulsé, étaient utilisés et la puissance était ajustée selon une large plage de valeurs. Il y a également des lacunes quant à l'évaluation quantitative de la lésion RF et du dommage adjacent ainsi qu'au niveau des concepts biophysiques qui expliquent les mécanismes de la perforation RF.

CONCEPTS DE BASE DE LA PERFORATION RADIO FRÉQUENCE

La perforation RF implique la destruction du tissu au voisinage d'une électrode possédant un potentiel électrique élevé. La technique RF utilise un courant alternatif de 100 kHz à 3 MHz, qui ne stimule ni les muscles, ni les terminaisons nerveuses, ce qui permet d'opérer sans anesthésie générale. Le courant RF circule dans le cathéter, du générateur vers une mince électrode active, puis à travers le tissu vers une électrode indifférente rattachée au générateur. Le tissu, comme toute matière, offre une résistance à la circulation du courant. L'énergie électrique se transforme en chaleur lorsque les ions entrent en collision entre eux et avec les molécules. La chaleur accumulée augmente la température du tissu : à 49° C, la coagulation du tissu a lieu; à 70° C, le tissu commence à se

dessécher; à 100° C, l'ébullition de l'eau à l'intérieur de la cellule augmente la pression interne, provoquant l'explosion de la membrane cellulaire. Ce dernier mécanisme de destruction du tissu s'accompagne de production de vapeur et de petites bulles d'air, et est présentement reconnu comme étant le principal mécanisme de destruction du tissu. Ce mécanisme est non-linéaire parce qu'il survient lorsque la température du tissu dépasse le seuil de 100°C, et nous le nommons « rigidité thermique » par analogie avec la rigidité diélectrique.

Cependant, la perforation avec un courant RF continu produit une coagulation négligeable, tandis que celle avec un courant RF modulé ou pulsé produit une hémostase considérable, non désirée, malgré l'utilisation de la même puissance appliquée. De plus, l'effet de dessiccation du tissu à 70° C peut empêcher la circulation du courant à cause de l'augmentation d'impédance. Afin de comprendre la nature de ces observations, nous avons examiné un autre effet de l'interaction entre la cellule et le champ électrique : le mécanisme de l'électroporation. L'électroporation est un mécanisme non linéaire de nature électrique, qui consiste en la formation de larges pores aqueux à travers la membrane cellulaire lorsque le voltage transmembranaire induit par le champ électrique dépasse un certain seuil. La formation de ces pores entraîne une augmentation de la pression intracellulaire à cause de l'entrée d'eau causée par le gradient de pression osmotique. Ce gonflement osmotique peut provoquer la rupture de la membrane. L'étendue de l'électroporation dans le tissu est proportionnelle au champ électrique et peut être évaluée quantitativement. Le voltage transmembranaire critique de l'électroporation pour la cellule myocardique est d'environ 450 mV pour une impulsion de 5 msec.

Le claquage, une caractéristique accompagnant la perforation RF, a été observé lors de nos expériences *in-vitro* et est décrit dans la littérature. La formation des étincelles a lieu dès le début de la formation du canal et est liée à la transmission du courant à travers une couche de vapeur dans un champ électrique élevé. Des étincelles sont accompagnées par une augmentation d'impédance abrupte. La fréquence des étincelles

n'est pas connue de même que leur contribution à l'impédance de l'interface cathéter-tissu. Le claquage est un effet aléatoire qui ne peut pas être décrit par un modèle déterministe.

MODÉLISATION NUMERIQUE DE LA PERFORATION RADIO FRÉQUENCE

Pour étudier la perforation RF et l'influence de la géométrie de l'électrode et du voltage appliqué, un modèle numérique simple a été développé. Le modèle est basé sur le mécanisme de la rigidité thermique qui est considéré comme étant le mécanisme principal de la perforation RF. Le mécanisme de claquage, à cause de sa nature profondément aléatoire, a été exclu de notre considération en supposant un contact étroit entre l'électrode et la couche du tissu.

Le mécanisme de la perforation dans notre modèle numérique a été réduit à une simple règle : chaque fois que la température du tissu dans tous les éléments directement en face du cathéter dépasse 100° C, ceux-ci sont considérés comme étant immédiatement vaporisés et le cathéter avance au-delà de ces éléments. Ainsi, la règle qui contrôle le déplacement du cathéter dépend seulement de la température du tissu et non de l'électroporation. Cependant, l'étendue du tissu électroporé a été évaluée et comparée avec l'étendue du tissu réchauffé à 70° C afin de trouver le voltage optimal de la perforation RF.

Le modèle cylindrique est composé d'une couche du tissu (2mm d'épaisseur et 3.5 mm de rayon) entre deux couches du sang (1.2 et 0.2 mm d'épaisseur). Une électrode cylindrique (longueur de 0.7 à 2.4 mm ; rayon de 0.15 à 0.22 mm) est placée à angle droit avec le tissu, une électrode indifférente est placée à l'autre extrémité du domaine cylindrique vis-à-vis l'électrode active. Chaque couche du modèle est considérée comme étant isotrope et homogène. Le modèle tridimensionnel, puisqu'il posséde une symétrie axiale, a été réduit à un modèle bidimentionnel dans le plan *r0z*.

La méthode des différences finies a été employée pour discrétiser le domaine spatial (les éléments ont des côtés de 38 μm). Cette méthode permet de conserver le même maillage au fur et à mesure de l'avance du cathéter à travers du tissu. L'évolution temporelle de la température locale est définie par l'équation de bio – chaleur :

$$\frac{\partial T}{\partial t} = \frac{1}{\rho c}\left[\left(k\nabla^2 T\right) + c_b w_b \left(T_b - T\right) + P_d\right] \tag{C.1}$$

où c est le chaleur spécifique du tissu; ρ - la densité du tissu ; k - la conductivité thermique locale; c_b - le chaleur spécifique du sang; w_b - la perfusion du tissu par le sang; T_b - la température du sang (supposée constante); et P_d - la densité de la puissance dissipée. La densité de la puissance dissipée se calcule par l'équation suivante :

$$P_d = \frac{\sigma E^2}{2} \tag{C.2}$$

où σ est la conductivité électrique et E est l'intensité du champ électrique. Le champ électrique a été déterminé par le gradient du potentiel à partir de l'équation de Laplace sous l'hypothèse quasi – statique :

$$\nabla(\sigma_0 \nabla V) = 0 \tag{C.3}$$

ici σ_0 est la conductivité électrique à la température 25° C. L'algorithme des différences finies a été employé pour résoudre l'évolution temporelle de la température avec un schéma implicite ayant un intervalle temporel de 10 msec.

L'étendue du tissu électroporé a été évaluée par l'équation modifiée de Schwan :

$$V_m = \frac{a\, E_{ap}}{\left[1 + \left(2\pi f \tau_m\right)^2\right]^{1/2}} \tag{C.3}$$

où V_m est égal à 450 mV; E_{ap} est le champ appliqué obtenu à partir du gradient de la distribution du potentiel. L'étendue du dommage a été évaluée par l'équation d'Arrhenius :

$$\Omega = \int A \times \exp(-E_a / RT) dt \qquad \text{(C.4)}$$

où Ω est le dommage accumulé; A est le facteur de fréquence; E_a est l'énergie d'activation; R - la constante universelle des gaz; T - la température (°K); t - le temps.

RÉSULTATS NUMÉRIQUES ET EXPÉRIMENTAUX

La simulation numérique a permis de trouver le voltage critique, correspondant à la température de 100°C dans les éléments qui sont directement en face de l'électrode. Ce voltage critique est égal à 75 V dans le myocarde perforé par l'électrode Baylis et il correspond au voltage de perforation obtenu expérimentalement. Les impédances initiales, calculées numériquement et expérimentalement, coïncident assez bien.

Cependant, avec ce voltage critique, seulement la moitié des cellules réchauffées à 70 C ont été électroporées, ce que signifie une grande probabilité de formation de zone de tissu desséché. Un voltage de 100 V est plus approprié car il produit les mêmes étendues de tissu électroporé et réchauffé. Les expériences ont confirmé ces résultats de simulation : le cathéter a coincé dans le tissu pendant la perforation avec 75-80 V, tandis qu'une perforation rapide et propre a eu lieu avec un voltage de 100 V.

L'estimation de l'étendue du tissu endommagé a montré la même tendance que celle de l'électroporation : au début de la formation du canal, la zone du tissu endommagé diminue avec l'augmentation du voltage. Le dommage minimal au tissu adjacent a été observé expérimentalement avec un voltage de 100 V.

La simulation de la perforation RF avec les électrodes de différentes longueurs et différents rayons a montré que le début de formation du canal commence plus tôt avec une électrode si la longueur et le rayon sont plus petits. Le voltage critique diminue avec la diminution de la longueur ou du rayon de l'électrode.

Pour étudier l'influence de la forme de l'électrode, on a calculé la distribution du potentiel autour de l'électrode pour différents types de forme du bout : cylindrique, hémisphérique et bulbeuse. On a constaté que la forme optimale de l'électrode est hémisphérique, car elle produit un champ uniforme qui peut minimiser la formation des étincelles et le réchauffement excessif du tissu par rapport aux autres électrodes.

Le voltage critique de la perforation de la valve, calculé numériquement selon le modèle de rigidité thermique (35 V), ne se correspond pas au voltage de la perforation observé expérimentalement (65 V). Il est possible qu'un ou plusieurs autres mécanismes puissent jouer un rôle dans la destruction du tissu valvulaire, en plus du mécanisme de rigidité thermique. L'effet d'électroporation dans la valve n'est pas décrit dans la littérature.

DISCUSSION, CONCLUSION

Notre étude a permis d'améliorer la compréhension des différents phénomènes physiques qui sont mis en jeu lors de la perforation RF du tissu cardiaque. Le modèle numérique de perforation RF inclut deux étapes : le réchauffement du tissu et la formation du canal à travers le tissu. Dans ce modèle, le déplacement du cathéter n'obéit pas aux mécanismes d'électroporation et de claquage.

Les simulations numériques ont permis de déterminer le voltage critique de la perforation RF du myocarde. Les calculs de l'étendue du tissu électroporé et du dommage accumulé ont permis de déterminer un voltage optimal qui produit une dessiccation négligeable, un dommage latéral minime, et une augmentation d'impédance minime. Le

calcul de la distribution du champ électrique a permis de déterminer la forme optimale de bout du cathéter. La simulation numérique de la perforation RF de la valve (basée sur le modèle thermique simple) n'a pas permis d'identifier correctement le voltage critique.

Des études futures pourront inclure :

- la simulation de la perforation RF de la valve cardiaque ;
- la simulation de la perforation RF du tissu par un cathéter coaxial ;
- l'incorporation des mécanismes d'électroporation et de claquage dans l'avance du cathéter à travers le tissu.

TABLE OF CONTENTS

LIST OF TABLES

LIST OF FIGURES

LIST OF SYMBOLS

I	Current (A)
V	Potential (V)
∇V	Gradient of potential (V/m)
V_m	Transmembrane voltage (V)
R	Resistance (Ω)
σ	Electrical conductivity (S/m)
E	Electrical field (V/m)
E_{ap}	RMS electrical field (V/m)
J	Current density (A/m^2)
f	Frequency (s^{-1})
q	Charge ($coulomb$)
$\vec{B}$	Magnetic flux density (T)
$\vec{v}$	Charge velocity (m/s)
μ	Charge mobility ($m^2/V/sec$),
n	Charge concentration (number in m^3)
$\vec{F}$	Force (N)
W	Energy generated by heating (J)
P_d	Dissipated power (W/kg)
SAR	Specific absorption rate (W/kg)
T	Temperature (^oC) (^oK);
ρ	Density (Kg/m^3)
c	Specific heat ($J/Kg\cdot^oC$)
c_b	Specific heat of blood ($J/Kg\cdot^oC$)

k	Thermal conductivity ($W/(m \cdot ^{o}C)$)
w_b	Blood perfusion ($Kg \cdot m^{-3} \cdot s^{-1}$)
h_t, h_b, h_i	Heat transfer coefficient of myocardium, blood, insulator ($W/m^{-2} \cdot s^{-1}$)
Ω	Accumulated damage (dimensionless)
E_a	Activation energy ($J \cdot mol^{-1}$)
A	Frequency factor (s^{-1})
t	Time (s)
t_m	Relaxation time of the membrane (s)
S	Area (m^2)
R_{cell}	Radius of cell
a	Half-length of cardiac cell (m)

CHAPTER I

INTRODUCTION

We intend to study the RF perforation of the pulmonary valve or the atrial septum in the case of pulmonary atresia with intact ventricular septum and other related pulmonary valve malformations or closures.

1.1 MORPHOLOGICAL FEATURES OF PULMONARY ATRESIA WITH INTACT VENTRICLE

Pulmonary atresia with intact ventricular septum is characterized by complete obstruction to forward blood flow from the right ventricle into the pulmonary trunk because the pulmonary valve is imperforated and the ventricular septum is intact. Right atrial blood leaves the right atrium via the foramen ovale (fetal opening between the two atria) and the pulmonary circulation is supplied via the patent ductus arteriosus (fetal junction between the pulmonary artery and aorta). Cases of pulmonary atresia with intact ventricular septum tend to fall into two groups, depending on the size of the right ventricular chamber, which, in turn, depends on the state of the tricuspid valve (PERLOFF, 1987).

1. Common variety: the right ventricular cavity is diminutive and thick walled, the tricuspid valve is competent in spite of some hypoplasticity of the valve (Fig.1.1). Intramyocardial sinusoids are important features in the presence of a small right ventricle (RV). Systolic pressure or isovolumic contraction forces blood from the cavity of the RV into the intramural space and hence into the coronary arteries, establishing the sinusoidal-

to-coronary arterial connection. Myocardial sinusoids communicate with coronary arteries or end blindly. Sinusoids that end blindly are exposed to a high systolic pressure without effective decompression via coronary arterial connections. Progressive sinusoidal enlargement culminates in myocardial rupture. Diastolic flow from the aortic root into a coronary artery and then into sinusoids and the right ventricular cavity potentially functions as an ischemic "steal" from the capillary bed, and myocardial infarction follows shortly.

2. Less common variety: the right ventricular cavity is of normal size or enlarged and thin-walled (Fig1.2). The tricuspid valve is deformed and incompetent.

In both cases the blood flow from the right ventricle into the pulmonary trunk is, by definition, impossible. Venous blood reaches the systemic circulation via the interatrial communication or through sinusoids. Oxygenated blood in the left atrium mixes with the unsaturated blood coming from the right atrium. This mixture flows into the left ventricle and aorta. Some blood from the aorta enters the pulmonary circulation via normally formed ductus arteriosus, upon which tenuous survival depends. Pulmonary flow is usually deficient and a comparatively small amount of oxygenated blood is available for mixing in the left side of the heart, which results in some level of cyanosis. When the ductus closes, effective blood flow into the pulmonary bed stops, and death follows shortly.

Over half of the patients die in the first month of life; the majority dies in the first three months, and very few live beyond their first year. Survival depends on the size of the interatrial communication and the patency of the ductus arteriosus. Some can survive more than a year because of the good-sized congenital communication between the aortic root and pulmonary trunk and large atrial septal defect.

The structure of the pulmonary obstruction in cases of pulmonary atresia with intact ventricular septum is similar to the critical pulmonary valve stenosis, the pulmonary atresia with ventricular septal defect and Tetralogy of Fallot (PERLOFF, 1987). The pulmonary atresia may include muscular, fibromuscular and valvular (membranous) tissues.

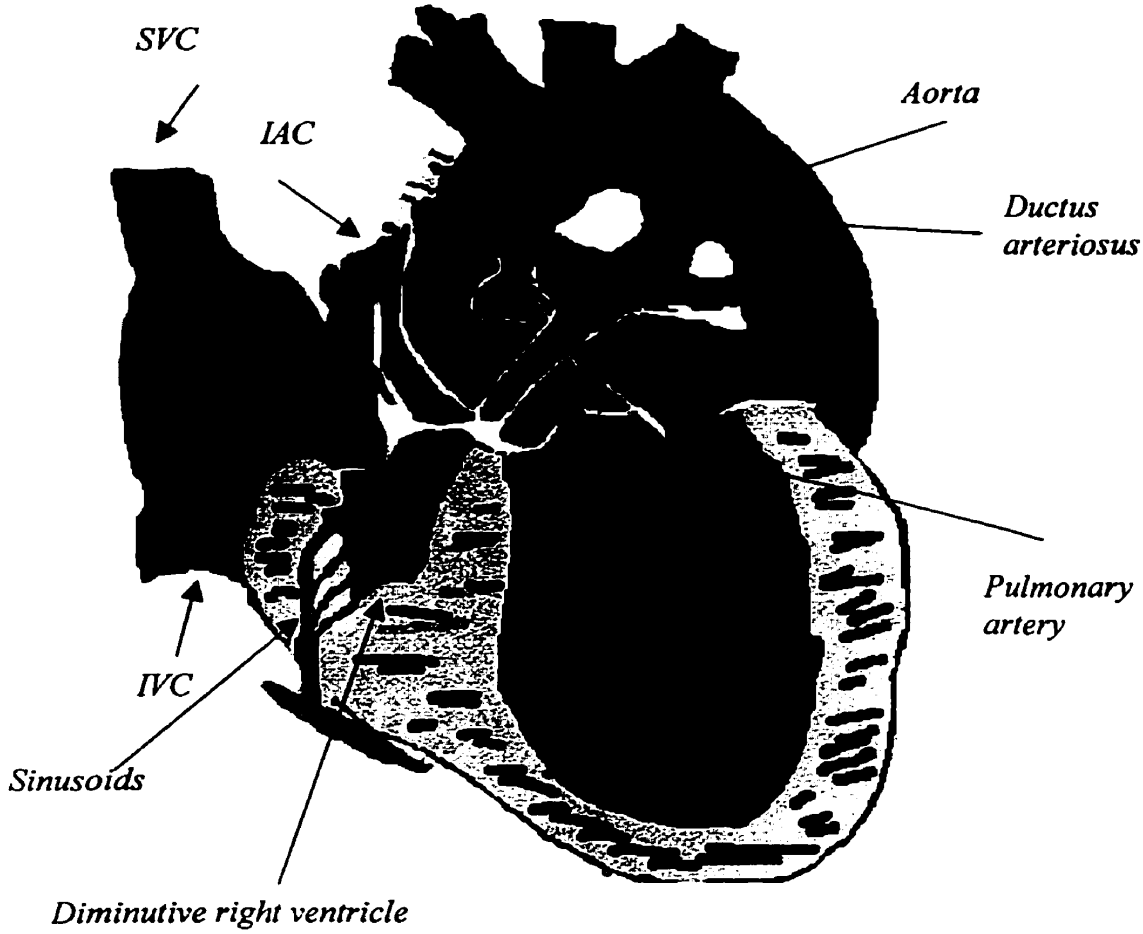

Figure 1.1. *Pulmonary atresia with intact ventricular septum, common variety.*
IVC - inferior Vena Cava; SVC - superior Vena Cava;
IAC - interatrial communication or the foramen ovale.

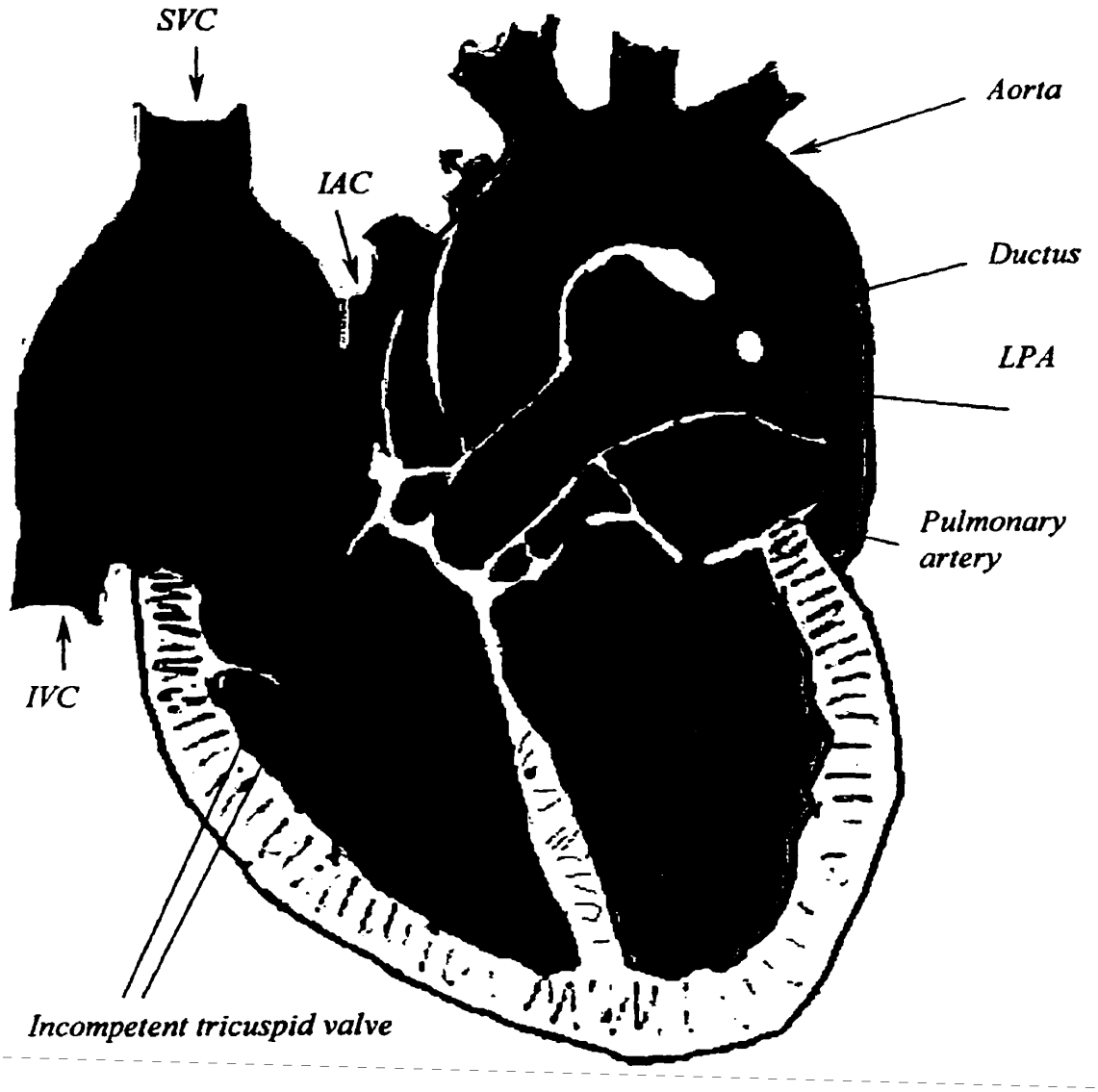

Figure 1.2. *Pulmonary atresia with intact ventricular septum, less common variety. IVC - inferior Vena Cava; SVC - superior Vena Cava; LPA - the left pulmonary artery; IAC - the interatrial communication.*

1.2 SURGICAL VERSUS RADIO FREQUENCY TREATMENT OF PULMONARY ATRESIA

Surgical treatment often remains unsatisfactory, especially in infants with hypoplastic arteries. Moreover, palliative surgery inevitably results in a postoperative scar formation, including some distortion of the pulmonary arteries (SCHNEIDER ET AL., 1995).

Recently, a radio frequency (RF) perforation technique has been used to perforate the atretic tissue (FONTES ET AL., 1995; GIUSRI ET AL., 1996; HAUSDORF ET AL., 1993; HOFBECK ET AL., 1994; HOFBECK and SCHNEIDER, 1993). The 2F cerebral "Osypka" catheter was used in an unipolar fashion. Monopolar current with a 500 kHz frequency from the 200 HAT-S generator (OSYPKA) was delivered to the heart via the catheter tip. The return electrode, placed on the torso, provided a path for return of the high frequency current to the generator.

Anatomy of the cyanotic heart disease varied from case to case: pulmonary atresia with the intact ventricular septum or with the ventricular septal defect; critical valvular pulmonary stenosis with the intact ventricular septum, Tetralogy of Fallot. Muscular, fibromuscular and membranous tissues were perforated in order to recanalise the pulmonary artery.

However, technical data mentioned in all protocols of the RF perforation were incomplete and varied from one perforation to another, depending mostly on the applied power, current waveform, tissue type, etc. The shape and length of the electrode were not specified. Applied power was adjusted in order to attain final perforation in course of the electrosurgical procedure, especially when current was delivered in short pulses (see Table 1.1).

Tissue	Current	Power
Muscular	Continuous	5-12 W
	Pulsed	4-20 W
Membranous	Continuous	14-28 W
	Pulsed	5-50 W

Table 1.1. *Summary of the electrosurgical procedures performed with the 2F catheter OSYPKA.*

Such variety of power settings, as well as the presence of two different types of current waveform indicates a lack of knowledge about RF perforation. There is a general lack of quantitative assessment of the lesion and damage to the adjacent tissue. Hence, the medical authorities do not recommend this procedure for general use (HOFBECK ET AL., 1994).

CHAPTER II

RADIO FREQUENCY PERFORATION: GENERAL CONSIDERATIONS

In the field of electrosurgery, RF perforation is regarded as a cutting procedure, which implies a complete destruction of some tissue layer in direct contact with the electrode. Like RF ablation, RF perforation is basically a thermal phenomenon. However, the exact mechanisms underlying this "cutting" lesion have not yet been specified (PEARCE, 1986; DUFFY AND COBB, 1995).

2.1 MECHANISM OF RADIO FREQUENCY HEATING

The RF technique uses a high frequency alternating current, usually from 100 kHz to 3 MHz. The current flows from the high frequency generator to the active electrode, then through the tissue and back to the generator via an indifferent electrode. The tissue, like all other physical substances, offers resistance to the flow of electrical current. As the charged particles (ions) constituting the current attempt to move through the tissue, they constantly collide with the molecules of the tissue, as well as with themselves. Through these collisions, electrical energy transforms into heating as dictated by Joule's law:

$$W = I^2 \cdot R \cdot t \tag{2.1}$$

where W is the generated heat (*joule, J*); I, the current (*ampere , A*); R, the resistance (*ohm*); t, time.

This energy dissipates in the tissue. The density of the dissipated power (P_d) in a homogeneous, isotropic region with an alternating sinusoidal current is calculated as (Appendix):

$$P_d = \frac{J^2}{2\sigma} = \frac{\sigma E^2}{2} = \frac{\sigma (\nabla V)^2}{2} \tag{2.2}$$

where J is the current density (A/m^2), σ is the electrical conductivity of tissue ($S*m^{-1}$), E is the electrical field (V/m), and ΔV is the voltage gradient (V/m).

During lesion formation, heat is lost from the tissue via conduction (heat diffusion) to the adjacent regions and via convection through blood perfusion or to the environment (blood / air). The heat accumulated in the tissue is the difference between the generated heat and heat losses. The tissue temperature rise depends on the accumulated heat which is determined by the current density and the tissue conductivity.

2.2 CURRENT DISTRIBUTION IN TISSUE

2.2.1 Electrical resistance of tissue

In the radio frequency range, biological medium can be regarded as a purely resistive and isotropic medium (Appendix). Different tissues have different electrical conductivities, which modify the current flow. The high conductivity regions such as the introventricular blood masses can become the preferred current pathway and carry disproportionate amount of current. In addition, as tissue dries out or is desiccated, its resistance increases greatly and the current decreases. Moreover, the tissue conductivity increases with temperature because of the ionic nature of the tissue. The electrical conductivity as a function of temperature can be expressed as:

$$\sigma (T) = \sigma_0 \exp \left[0.02 * (T - T_0) \right] \tag{2.3}$$

where σ_0 is the conductivity at temperature T_0, σ is the conductivity at temperature T (degrees Celsius).

2.2.2 Current density

Current density in tissue depends on the applied current and the geometry of the current distribution. The best cutting action is achieved when applying an unmodulated continuous sine wave current, thus providing continuous energy delivery to the tissue (Fig.2.1-A). This waveform further can be modulated to achieve a combined cutting and coagulating action by damping segments of the sine wave (Fig.2.1-B). The coagulating effect increases as the modulation increases. When the combined sine wave and the interrupted (coagulating) waveform are used for cutting (Fig.2.1-C), the coagulum layer extends deeper into the tissue under the desiccated layer (DUFFY AND COBB, 1995; PEARCE, 1986).

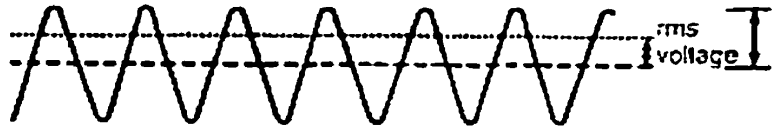

A - cutting waveform

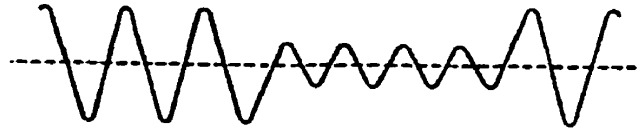

B – damped (blended) waveform

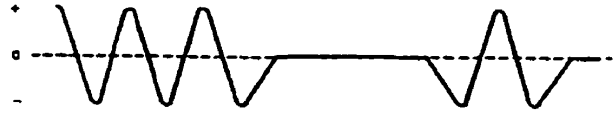

C – interrupted (coagulating) waveform

Figure 2. 1. *Examples of current waveforms used in electrosurgery.*

The current distribution is defined by the current source and sink geometry, their relative position with respect to the tissue and by the conductive environment. For any applied current, an electrode with a smaller contact surface will develop a higher current density in the adjacent tissue, and cutting action can occur more efficiently.

Current may be delivered to the tissue in monopolar or bipolar fashion. Monopolar current is delivered via the active electrode and is collected with the indifferent electrode (Fig.2.2-A). The surface of the active electrode is relatively small, resulting in high concentration of current at the active electrode-tissue interface. The passive electrode has a proportionally much larger surface compared to the active electrode. Thus, the current density in the tissue in vicinity of the passive electrode is small. With the alternating current, the active and passive electrodes are both source and sink. Since the current flows from one electrode to another with a high concentration around the small active electrode, the desired effect is localized at this area.

In a bipolar arrangement (Fig.2.2-B) current flows mainly through the volume of tissue between the poles of the electrodes, and not through the other part of the patient's body. This allows to reduce the power level. The current distribution is generally symmetrical about the centerline between the poles.

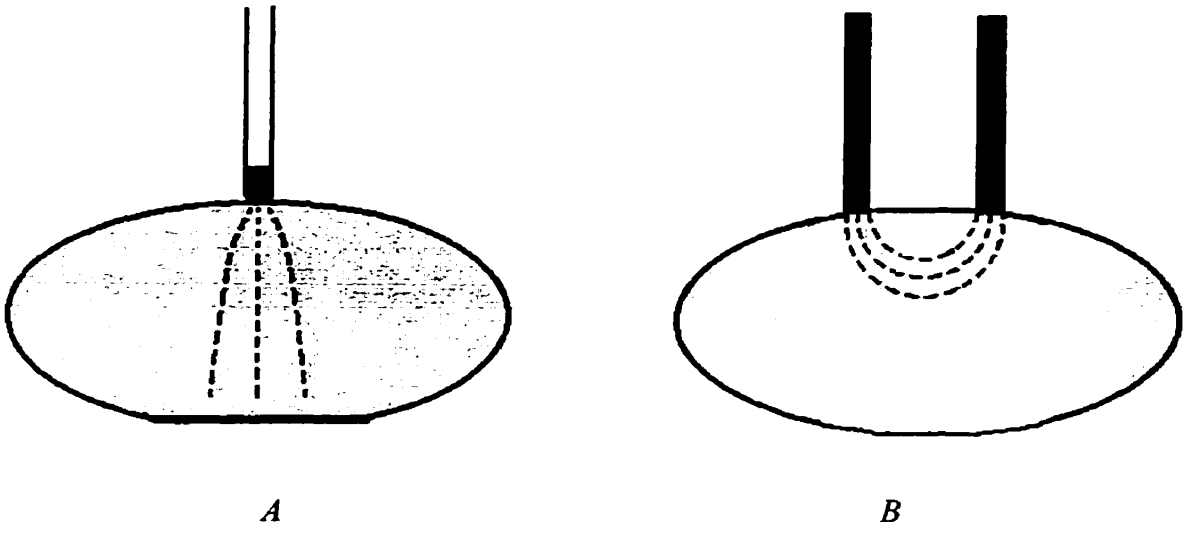

Figure 2.2. *A) a monopolar tissue-electrode arrangement: current flows between the active and grounded electrodes; B) a bipolar tissue-electrode arrangement: current flows between two poles.*

2.3 THERMAL EFFECT IN TISSUE

Different changes occurring in the tissue that are caused by heat depend on the tissue temperature and the duration of heat exposure. Slow heating with a low amount of applied power produces desiccation under the active electrode when the temperature reaches about 70°C. The deeper tissue layers at lower temperature will be coagulated. On the other hand, fast heating with high applied power results in intracellular boiling and instant vaporization. The pressure of the microscopic steam bubbles literally explodes the cellular walls. The tissue overheated above 200°C is carbonized.

CHAPTER III

BASIC CONCEPTS OF RADIO FREQUENCY PERFORATION

The radio frequency perforation is a complex phenomenon involving interactions between thermal breakdown, electrical breakdown and mechanical breakdown.

3.1 THERMAL BREAKDOWN

Our theoretical model of RF perforation is based on numerous experimental observations. From the cutting electrosurgical procedure performed mostly in gastroenterology and cancer surgery (BURLOW 1982; CURTISS 1973; HONIG, 1975), it is known that electrocutting occurs as a thin electrode contacts the tissue, allowing a high density current to flow through the tissue at the advancing edge. As a result of the high power density localized in the vicinity of the cutting electrode, the highest temperature is reached in the volume next to the electrode. The observation of steam and small bubbles of air at the electrode-tissue contact indicates boiling and vaporization occurring at above 100°C. The pressure increase resulting from the water phase change triggers the cell membrane rupture and the subsequent release of the cellular content. This cell disruption mechanism constitutes the thermal breakdown of the tissue.

This description of the thermal breakdown is rather idealistic. Alone, it does not explain many aspects of electrocutting. In order to achieve better understanding of the RF perforation some additional concepts were derived both theoretically and experimentally. These concepts imply that:

- the active electrode is thin (BURLOW 1982; CURTISS 1973; HONIG, 1975),
- a high current density flows through the cell at the advancing edge of electrode (CURTISS, 1973),
- the RF voltage should be relatively high (HONIG, 1975),
- the cutting speed has to be high (HONIG, 1975).

Since the current flows through the electrode-tissue interface, the current density is high if the electrode surface is small or the active electrode is thin. High current density in tissue results in high power density and generated heat. Fast temperature rise up to the water boiling point and the consecutive cell explosion result in high cutting speed.

One aspect of RF perforation that remains unexplained with the thermal breakdown model is the tissue desiccation in the vicinity of the catheter tip. When a cell is heated up to 70°C, well below 100°C, it dries out or desiccates (BARLOW, 1982). Desiccated tissue is difficult to cut, because there is less entrapped water to explode the cell, and also because the desiccated tissue has a greater resistance which diminishes the current (CURTISS, 1973). One can usually cut through a desiccated tissue using a higher power setting. However, the lesion looks like burning through the tissue with a hot wire. It is slow and heats a large volume of tissue. The effect of tissue desiccation complicates the thermal model of RF perforation. Another aspect that deserves a more thorough look is the "electrical field-cell" interaction, namely the structural changes induced by the electrical field itself.

3.2 ELECTRICAL BREAKDOWN: ELECTROPORATION

From our first experiments of RF perforation of the cardiac tissue *in-vitro*, we have found that RF perforation is a non-linear phenomenon which takes place only when voltage exceeds a certain level. Taking this into account, we reviewed the articles describing the " electrical field – cell " interaction, namely the effect of electroporation (KINOSITA, 1977; KNISLEY, 1994; KRASSOWSKA, 1995; TOVAR and TUNG, 1991; TSONG, 1991; WEAVER, 1993).

3.2.1 Mechanisms of electroporation

The cell membrane can be regarded as an insulator separating two conducting aqueous phases, i.e. as a dielectric in a parallel plate capacitor. Therefore, in an equivalent electrical circuit the cell membrane can be represented as a capacitance and a resistance arranged in parallel. Like any material, the membrane will become polarized in the presence of an electric field. Polarization most often occurs due to the formation of dipoles or the reorientation of permanent dipoles within the membrane and the electrolytic solution. Orientational polarization occurs in a dielectric containing polar molecules with a permanent dipole as in the case of a biological membrane. These dipoles normally may be randomly oriented but align themselves in the direction of the field lines in the presence of an electric field to an extent that depends on the field strength and the thermal agitation (ZIMMERMANN, 1982). Under a rapidly changing or an alternating field of high frequency, fewer dipoles will be formed or reoriented and consequently, a dielectric dispersion will occur. In the frequency range where dispersion occurs, the dielectric absorbs energy from the electrical field (β - dispersion for 500 kHz). With increasing frequency, the dielectric constant and the specific resistance often decrease.

If the cell is subjected to a high electrical field of the order of several kV/cm, voltage sensitive protein channels will be opened. However, opening of these channels may not be sufficient to prevent the continuous increase of the transmembrane potential V_m to reach the breakdown potential of the lipid bilayer. A dramatic increase of the conductance and permeability of cell membranes can be observed as due to aqueous pore formation - *electroporation* - in the lipid bilayer with current passing through all the channels.

This field-induced increase of permeability has been termed *electrical (dielectric) breakdown* because of the massive loss of the membrane insulation property. In solid-state physics, the phenomenon of dielectric breakdown implies an irreversible change in the structure, whereas in the case of a biological membrane, the change is reversible

without any adverse side effect as long as the exposure time is not too long and the field intensity is not too high.

The molecular processes leading to pore formation following the electrical breakdown are still unknown. The polarization of the membrane dielectric material and the orientation of the permanent and induced dipoles in the electrically anisotropic molecules within the membrane in response to a strong electric field pulse can cause local tension and mechanical instabilities which would ultimately bring about the formation of pores in the lipid bilayer. Several authors consider the local electro-mechanical compression of the membrane as a possible mechanism for the reversible electrical breakdown. There is strong evidence that the membrane can be compressed by at least 10% (in the voltage relaxation studies). It is probably feasible that this 10% decrease in the thickness of the membrane or its part by the compressive force triggers other processes which ultimately lead to breakdown (WHITE, 1974).

Furthermore, Benz et al. (BENZ et al., 1979) have shown that this degree of compression could lead to the situation where the energy of the ions in the electrical field could reach the energy required to inject ions from the aqueous phase into a thin layer.

Finally, the avalanche production of charge carriers could also be considered as a possible mechanism for electrical breakdown in the biological membrane (COSTER, ZIMMERMANN, 1975). Because of the non-crystalline nature of the cell membrane, it seems unlikely that this effect would be primarily responsible for the breakdown, although it is conceivable that some structured changes emerge in the way of certain electromechanical precompression of the membrane, favoring a mechanism of this nature.

3.2.2 Aqueous pores formation with dielectric breakdown

The transmembrane potential induced by an applied electrical field for a round cell (SCHWAN, 1983) is expressed by:

$$V_m = \frac{1.5 * R_{cell} * E_{ap} * \cos\theta}{[1 + (2\pi * f * \tau_m)^2]^{1/2}} \qquad (3.1)$$

Where θ is the angle between the applied field and the point of interest on the membrane surface; R_{cell} is the cell radius, E_{ap} is the RMS applied electrical field; τ_m is the relaxation time of the membrane or the rise time of V_m, f is the frequency.

The transmembrane voltage induced by an electrical field depends on the cell size and shape, the applied electrical field strength and the type of applied current (direct versus alternating current). For a cylindrical cell, the equation 3.1 changes to:

$$V_m = \frac{F(a/b,\theta) * a * E_{ap} * \cos\theta}{[1 + (2\pi * f * \tau_m)^2]^{1/2}}, \qquad (3.2)$$

where $F(a/b, \theta)$ is a coefficient that depends on the ratio between the cell half-length and half-width and a is the cell half-length (equation 3.1 modified by KINOSITA and TSONG, 1977). The relaxation time of membrane depends on the cell size and shape: for biological cells of diameters in micrometers, t_m is less than 1 μsec, while for the larger ceiis t_m is greater than 1 μsec.

Aqueous pores are formed in the lipid membrane if the transmembrane potential reaches a critical level leading to electroporation (usually between 500 mV to 1 V). The time required for the pores to open is less then 30 μsec for the critical transmembrane voltage. Visual (optical range) observations have shown that mechanical rupture of the membrane begins from a single point. Chang and Reese (1990) have detected these

electrically generated pores by means of electron microscopy and conjectured that their density can be a function of the applied field.

The transmembrane voltage leading to the dielectric breakdown depends on temperature. Between 4°C and 30°C the critical membrane potential decreases from 1200 mV to 600 mV in the presence of 1 M of KCl. The applied electrical field intensity that reaches the reversible cell breakdown is greater for shorter duration of the electrical field pulse.

3.2.3 Conduction through aqueous pores in lipid bilayer and protein channels during the dielectric breakdown

Once a current I is induced in a defect, $I^2*R*\Delta t$ of heat is generated (R is the resistance of the defect, Δt is the duration of electrical field application). The local heating could cause a phase transition or disordering of the lipid layer (LOPEZ, ROLS, 1988). Weaver (WEAVER, 1993) has calculated the extent of local heating using the estimated values of effective transmembrane potential, conductivity of the medium and pore size. A local temperature rise of several degrees may be reached in micro to milliseconds. If Δt is a few milliseconds or longer, the current could also produce electroosmosis effects, thus mechanically enlarging the defect (pore $\approx$ 40 nm).

Part of the energy increases the pressure inside the cell above the osmotic level. This leads to cell swelling as the pressure from the outside is transferred to the cytoplasm. Kinosita and Tsong (1979) have found that the cell lysis is due to the colloidal osmotic pressure of the cytoplasmic macromolecules. The kinetics of swelling due to water uptake and the establishment of the Donnan's equilibrium for the ions depend on the ratio of the field-induced membrane pore radii and change of the external molecules (See Fig.3.1 (TSONG, 1991)).

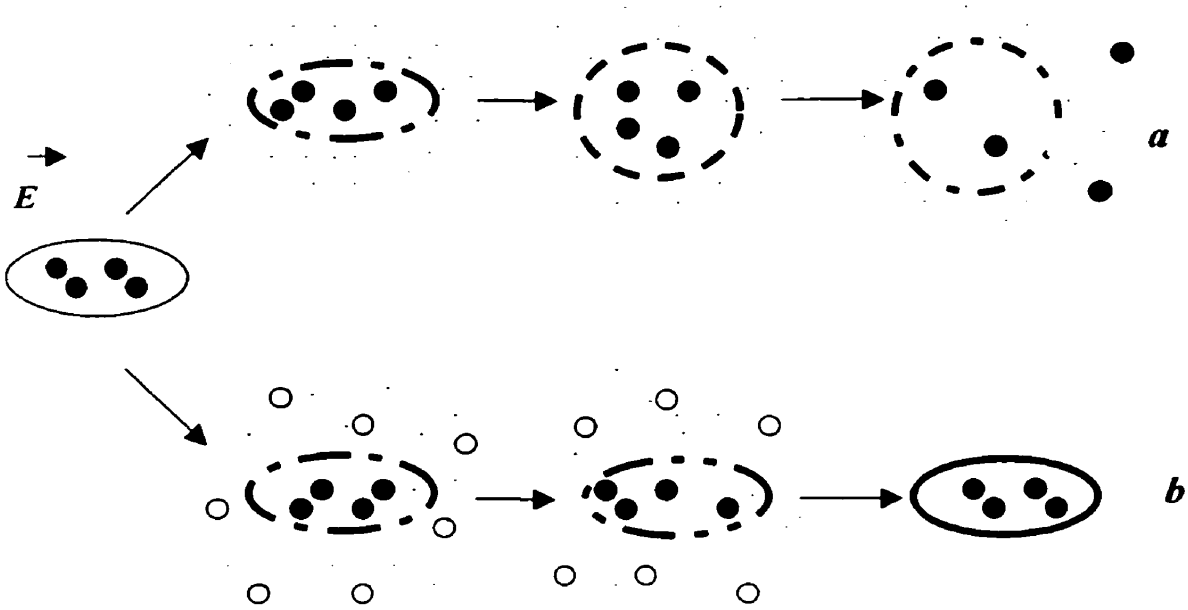

Figure 3.1. *Electroporation and resealing of the cell membrane; a – cell swelling, colloidal osmotic pressure drives the influx of water and small solutes; b – cell resealing, due to the balance of colloidal osmotic pressure of the cytoplasmic macromolecules by the molecules which are larger than the size of electropores.*

Reversible opening/closing of a protein channel occurs in the microsecond time range. Protein channels once opened may experience a current much larger than they are designed to conduct As a result, these channels can be irreversibly denatured by Joule heating or electric modification of their functional groups. This kind of protein denaturation takes place in milliseconds to seconds (KIM, BALDWIN, 1982). Pores in the lipid domain are expected to reseal in milliseconds to seconds (BENZ, ZIMMERMANN, 1981; TEISSIE, TSONG, 1981).

3.2.4 Dielectric breakdown and cell lysis

The electrical breakdown leading to death of a cell depends on two parameters:

- the applied electrical field, which exceeds the critical field of membrane to create holes,
- and the Joule energy deposited in the membrane, which must exceed the minimum value beyond which the cell can not recover.

The first parameter initiates the reversible breakdown and the second one controls the irreversible electrical breakdown leading to cell death.

Cell lysis can be prevented by balancing the colloidal osmolality of the cells with molecules larger than the size of the electropores. This procedure stops cells from swelling and greatly facilitates membrane resealing. An excess of such divalent cations as Mn^{2+}, Ca^{2+}, Ba^{2+}, Mg^{2+}, Zn^{2+} inhibits cell lysis because of the interaction of such ions with phosphatidylserine exposed at the cell surface by the electrical breakdown and resealing in turn of the aqueous pores formed by the critical field. An excess of Na^{+} and K^{+} facilitates the cell lysis immediately at breakdown (SONG et al, 1993).

Cell lysis accelerates with increase of the electrical field intensity. As the electrical field increases, the percentage of participating cells increases as well, but the percentage of surviving cells simultaneously decreases. Eventually, for very large fields, there are no surviving cells. This could be explained by the increase of aqueous pore density (several locally separated breakdown centers), the fast enlarging of formed pores, and the fast denaturation of protein channels. Since cell osmosis and cell lysis depend on Joule heat deposited to a cell, they depend on pulse duration as well. Hemolysis by a 10 μsec pulse was more than 10 times faster than that by a 5 μsec pulse. Further increase in pulse duration, however, slowed down the reaction.

When the number of pulses is increased while keeping the other conditions constant, the degree of killing increased rapidly at first, and then more slowly. When the length of pulse was shortened, more pulses were required to achieve the same degree of killing. If these two effects were combined, it was found that the degree of killing appears

to be related to the product of the number of pulses and the pulse length, that is, to the total time for which the voltage is actually applied to the cell. Because of the short time of the pores resealing (from micro to milliseconds), the pulsated electrical field must be applied in long pulses with short intervals between the pulses to maximize the temperature rise or irreversible breakdown (SALE and HAMILTON 1967).

3.2.5 Electroporation of the cardiac tissue

Electroporation was observed during application of the defibrillation shocks (TOVAR, TUNG, 1991) and has been numerically simulated for a one-dimensional model of cardiac strand (KRASSOWSKA, 1995). For the applied electrical field of 2 kV/m (ramp pulses of 7 msec) it was found that electroporation took place only in the vicinity of the electrode tip. Numerical simulation with the same electrical field has shown that only the part of the first cell in contact with the electrode was electroporated. An electric field of 5 kV/m was strong enough to produce breakdown of one cell. As the electrical field amplitude increased up to 12 kV/m, several cells of the cardiac strand closest to the electrode underwent electroporation (KRASSOWSKA, 1995). The reversible membrane breakdown took place when the transmembrane potential attained about 450 mV in the case of 5- and 10-ms rectangular pulses (TOVAR, TUNG, 1991).

Figure 3.2 shows the strength-duration relationship of electroporation for the cardiac cell in case of monophasic voltage pulses (TOVAR, TUNG, 1991).

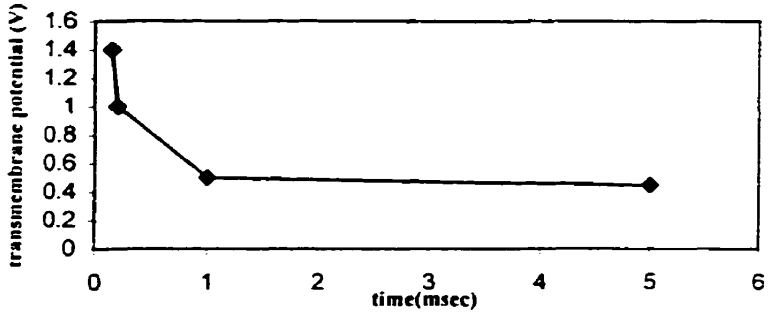

Figure 3.2. *The strength-duration relationship of electroporation for the cardiac cell in case of monophasic voltage pulses (TOVAR, TUNG, 1991).*

3.3 ARC

Another effect that merits our attention is arcing at the electrode-tissue interface. In our experiments as well as in others (AN et al., 1989; DUFFY and COBB, 1995; PEARCE, 1986; TUCKER ET AL., 1992; TUCKER ET AL., 1984) arcing was always observed during successful RF perforation attempts. An arc is the result of current transmission through a thin vapor layer between the electrode and the tissue. Ionization of this layer is due to the high electrical field (dielectric breakdown). For a sinusoidal alternating current, the ions form a cascading amplification through collisions, until critical density of the ion cloud is reached. Then, the impedance between the electrode and the tissue falls, the current flows and the ions give off light (arc), relaxing to a lower density. The arc impedance in tissue was measured by different researches (AN ET AL., 1989; TUCKER ET AL., 1984; TUCKER ET AL., 1992), as well as during our *in-vitro* experiments. An arcing event is identified by a rapid increase of impedance.

The arc occurrence and intensity depend mainly on the breakdown voltage, the vapor layer thickness, the concentration of residual ions from the previous discharges, the geometry of the active electrode tip and its contact with the tissue. The arc can be formed during each half-cycle if the electrical field is high enough to sustain ionization. If the sinusoidal current is continuous, there is very little time between the positive and negative half-cycles for the remnant of the ion cloud to dissipate. Thus, the ion cloud from the previous strikes favors additional strikes in the pathway of the previous arcs. A continuous sinusoidal waveform implies that the arc will form in a slightly larger cross section and will be slightly less intense than the arc formed by an interrupted waveform (AN ET AL., 1989; TUCKER ET AL., 1984; KELLY AND WARD, 1932). A coagulum formed at the electrode surface additionally contributes to the arc intensity and can impair the current flow.

Hence, the arc formation and the discharge location are quite random and cannot be approached with a deterministic model.

One potential danger of arcing is tissue stimulation, which can occur because of spurious current rectification induced by the intense arcing through the vapor layer (TUCKER ET AL., 1984). A low frequency current component can stimulate myocardium if its amplitude is higher than the threshold of excitability. The amplitude of the low frequency current is proportional to the arc intensity (TUCKER ET AL., 1984).

3.4 MODELING OF RADIO FREQUENCY PERFORATION

The process of RF perforation consists of two stages:

- local tissue heating up to 100°C before the onset of perforation;
- channel formation in the tissue with the catheter advancing through it.

The first stage encompasses tissue heating by the known current with known area of current distribution. The second stage includes tissue destruction by the thermal breakdown mechanism, but the current distribution is unknown because of the arcing

between the catheter tip and the tissue. Since arcing is a random phenomenon, the model of the second stage was simplified by assuming a close electrode-tissue contact without any intervening vapor layer. A possible consequence of this simplification may be an overestimated tissue damage with an overestimated speed of perforation.

Our model of RF perforation is based on the thermal breakdown mechanism, which is the main mechanism of tissue destruction with RF heating. The electrical breakdown or electroporation is an additional and necessary mechanism for RF perforation but it does not control the advancement of the catheter (perforation) in our model. However, the area of tissue undergoing electroporation can be compared with the area of tissue overheated to 70°C in order to estimate the continuation of perforation.

CHAPTER IV

Radio Frequency Perforation of Cardiac Tissue:

Modeling and Experimental Results

By:

Nelli Shimko, Pierre Savard *Biomedical Engineering Institute, École Polytechnique de Montréal and Université de Montréal, Centre de recherche, Hôpital du Sacré-Cœur de Montréal, Montréal, Québec, Canada.*

Kris Shah *Baylis Medical Company, Mississauga, Ontario, Canada.*

Submitted to Medical & Biological Engineering & Computing

ABSTRACT

Radio frequency (RF) current delivered through the tip of a thin catheter can be used to perforate the pulmonary valve or the atrial septum for the treatment of pulmonary atresia in newborns. To better understand the mechanisms of RF perforation, a numerical model was developed and experiments were performed. The axisymmetrical model consists of a cylindrical domain with a tissue layer between two blood layers. A potential difference is applied between the catheter tip and a large distant electrode. When the temperature produced by the current flowing inside the tissue exceeds 100°C in all the points that are directly in front of the catheter, these points are considered to be instantly vaporized and the catheter advances over these points. Experiments were also conducted in isolated canine cardiac tissue. The computed temperature time course coincided with measured temperature at small power settings. Simulated perforation occurred when the applied voltage exceeded 70-80 V in the myocardium, which also coincided with experimental observations. Shorter electrodes with smaller diameters produced a more rapid perforation. In conclusion, numerical simulations provide insights into such aspects of RF perforation as electrode size, current delivery, speed of perforation and collateral damage.

Keywords: pulmonary atresia, radio-frequency perforation, catheter, modeling

4.1 INTRODUCTION

Radio frequency (RF) perforation is used during the treatment of pulmonary atresia with intact ventricular septum, which is characterized by a complete obstruction to forward blood flow from the right ventricle into the pulmonary trunk because the pulmonary valve is imperforated. The morphology of this obstruction is similar to that of critical pulmonary valve stenosis, pulmonary atresia with ventricular septal defect or Tetralogy of Fallot (PERLOFF, 1987). Pulmonary atresia may include muscular, fibromuscular and valvular (membranous) components. The surgical treatment of the pulmonary atresia often remains unsatisfactory, especially for infants with hypoplastic arteries. Moreover, palliative surgery inevitably results in postoperative scar formation, including a distortion of the pulmonary arteries (SCHNEIDER et al., 1995).

Recently, RF current delivered through the tip of a thin catheter (cerebral, 2F) was used to perforate the atresia. A balloon catheter inserted through this perforation was then used to dilate the valvular lumen (HOFBECK et al., 1994; HAUSDORF and SCHNEIDER, 1993; FONTES et al., 1995; GIUSTI et al., 1996; HAUSDORF et al., 1993). Technical data such as the mode of current delivery (continuous versus pulsed), applied power (5-50 W), duration of energy delivery varied from case to case. Despite some clinical successes of RF perforation, both the related mechanisms and the effects of specific parameters such as the geometry of the electrode and the applied power damage remain unclear. Moreover, we are not aware of any modeling or *in vitro* experimental studies of RF perforation. The goal of the present study is to investigate the effects of

factors such as electrode geometry and applied voltage by developing a numerical model and by performing *in vitro* experiments in canine cardiac tissue preparations.

4.2 MECHANISM OF RF PERFORATION

In electrosurgery, RF perforation may be regarded as a cutting procedure, which is defined as a complete destruction of the tissue layers that are in direct contact with the electrode (PEARCE, 1986; HONIG, 1975). Experience in gastroenterology and cancer surgery (TUCKER et al., 1992; DUFFY and COBB, 1995; BARLOW, 1982) has shown that electrocutting occurs as a thin electrode contacts the tissue, allowing high density current to flow at the advancing edge. The conduction current generates heat in the resistive medium and increases the tissue temperature.

The increase of tissue temperature produces different effects. At 100°C, a "thermal breakdown" occurs: the pressure rise induced by the phase change of the water produces cell membrane rupture, release of the cell content and vaporization. At about 70°C, cells desiccate and proteins undergo a denaturation process. The desiccated tissue is more difficult to cut because there is less entrapped water to explode the cell and the lower electrical conductivity decreases the RF current (CURTISS, 1973). One can usually cut through a desiccated tissue by using a higher power setting, but the lesion is blackened, electrocutting is slower and a larger volume of tissue is damaged by heat.

In addition to "temperature–cell" interactions, "electrical field–cell " interactions must also be examined. Dielectric breakdown is a non-linear phenomenon that occurs when the intensity of the applied electric field exceeds a certain threshold and becomes high enough to ionize the medium. Electrical arcing can then occur and the dramatic increase of electrical conductivity increases the dissipated power and the tissue temperature. At the cellular level, dielectric breakdown can also manifest itself as electroporation (WEAVER, 1993; TSONG, 1991; KINOSITA and TSONG, 1977): the applied electrical field increases the transmembrane potential which in turn triggers the formation of aqueous holes through the lipid layer constituting the membrane. For example, the critical transmembrane potential for producing electroporation in cardiac cells is 400-500 mV for 5 msec monophasic pulses (TOVAR and TUNG, 1991; KNISLEY, 1994) and the corresponding electrical field ranges from 2.5 kV/m to 5 kV/m (KRASSOWSKA, 1995). Electroporation has different consequences: an excess current flows through the pores and generates heat; ionic diffusion through the pores increases the cell pressure above the osmotic level and leads to cell swelling, thus enlarging the holes. Thereby, electroporation contributes to cell destruction, as well as counterbalances cell desiccation.

An oscillating electrical field, transmitting energy through the tissue forces the cell membranes to undergo an oscillating motion which has the same effect as a localized sonication. Even when the amplitude of this oscillating motion is not high enough to result in mechanical breakdown, the alternating stress can still cause a structural fatigue and an increased susceptibility to electroporation. Summarizing these potential mechanisms, we conclude that RF perforation is a highly non-linear phenomenon

involving complex interactions between thermal breakdown, electrical breakdown and mechanical breakdown.

4.3 NUMERICAL MODEL

To investigate RF perforation and the influence of specific factors such as electrode geometry and applied voltage, a simplified numerical model permitting the computation of both the potential and the temperature distributions was developed. The mechanism of perforation in this model was reduced to the following rule: whenever tissue temperature exceeds 100°C for all the points that are directly in front of the catheter, these points are considered to be instantly vaporized, and the catheter advances one step forward over these points (Fig.4.1, bottom). Thus, the rule that applies to the displacement of the catheter depends only on tissue temperature and not on electrical criteria. The model assumes a close electrode-tissue contact with no steam layer and it does not incorporate complex factors such as electroporation, arcing and mechanical breakdown during catheter advance through the tissue layer.

The extent of the model is restricted to the vicinity of the catheter. The model consists of a cylindrical domain with a radius of 3,5 mm and an overall length of 3,5 mm (Fig.4.1, top). The basic model is constituted of a tissue layer (thickness: 2 mm) placed between two layers of blood (1,3 and 0,2 mm). This basic model also was modified to simulate some of the *in vitro* experiments by removing the two blood layers. The catheter axis coincides with that of the cylindrical block. The catheter is terminated by a

cylindrical electrode (length: 0,7-2,4 mm; radius: 0,15-0,22 mm) that is positioned at the right angle with the tissue. A large return electrode is located over all the bottom of the cylindrical domain. The size of the tip electrode (radius, length) and the properties of the tissue (myocardium, valve) are modified throughout our study so as to investigate the effects of these parameters.

Because of the axial symmetry, the potential and temperature distributions are computed in a two dimensional domain as a function of radius and depth (r and z). The finite difference method was used for both the potential and temperature computations because it allows keeping the same mesh as the geometry of the model changes to account for the displacement of the catheter inside the tissue layer. The mesh size was 38 μm (42,5 μm if the thermocouple was used instead of the catheter).

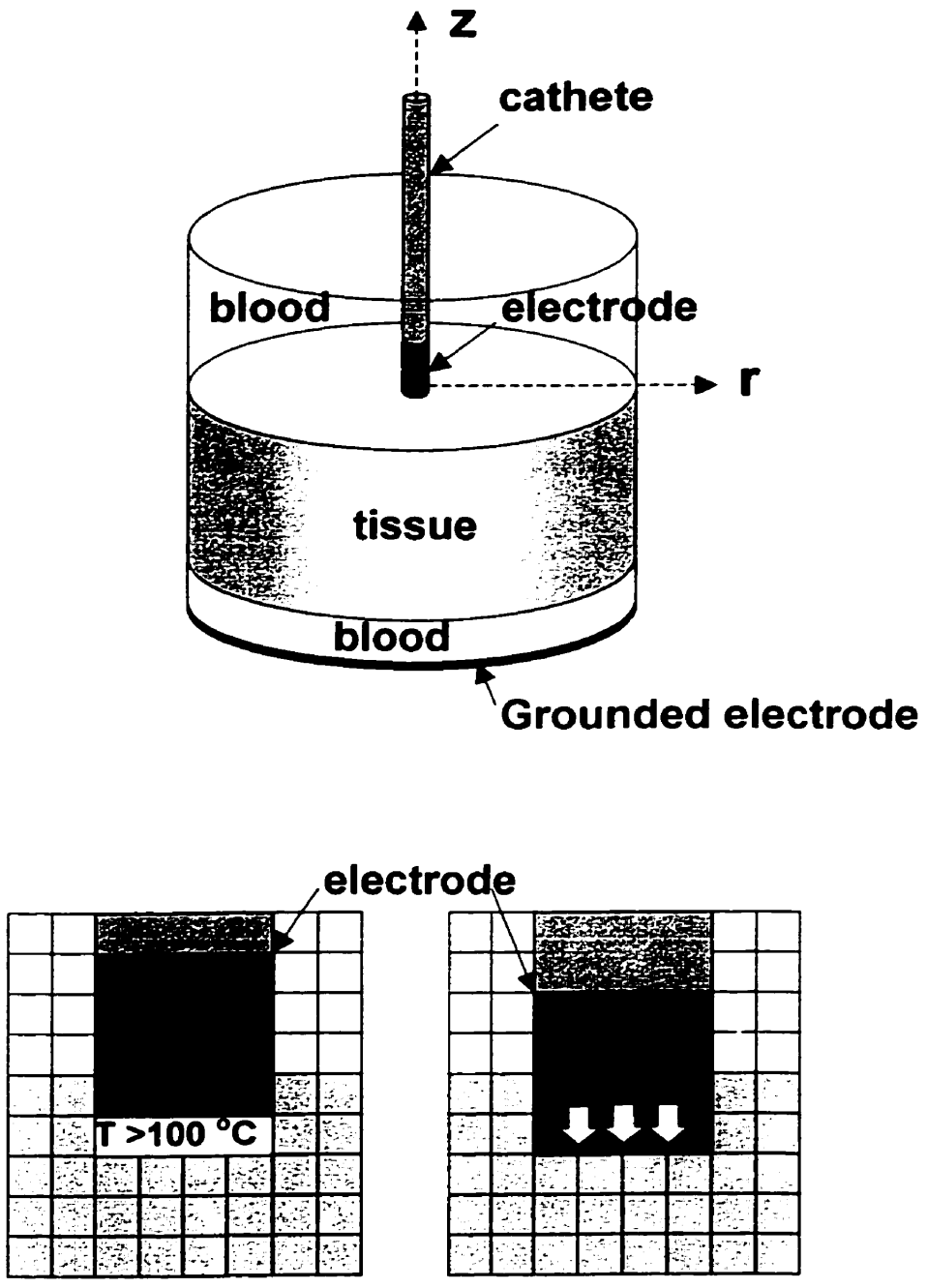

Figure 4.1. *The RF perforation model (cylindrical model consisting of a tissue layer placed between two layers of blood, the electrode is placed at right angle to the tissue)*

4.3.1 Potential computations

The RF current used for perforation has a frequency of about 500 kHz. At this frequency, the biological medium in the vicinity of the catheter can be considered as purely resistive and the electrical potential V in the tissue obeys the Laplace equation:

$$\nabla(\sigma_0 \nabla V) = 0 \tag{4.1}$$

where σ_0 is the local electrical conductivity at 25°C (the room temperature at which the experiments where performed). The boundary conditions are: constant potential over the tip electrode (V_0, expressed as a peak value in the Results Section); null potential over the return electrode; null normal component of the current density over the remaining lateral boundaries; continuity of the potential and the normal components of the current density at the blood-tissue interfaces.

4.3.2 Temperature computations

The rise of the local temperature T is governed by the bio-heat equation:

$$\frac{\partial T}{\partial t} = \frac{1}{\rho c}\left[\left(k\nabla^2 T\right) + c_b\, w_b \left(T_b - T\right) + P_d\right] \tag{4.2}$$

where c is the specific heat of the tissue; ρ, the tissue density; k, the local thermal conductivity; c_b, the specific heat of the blood; w_b, the blood perfusion provided by the

arteries; T_b, the blood temperature; and P_d, the dissipated power density. The first term within the brackets represents the transfer of thermal power by thermal conduction, the second term represents the transfer of thermal power by convection through local tissue perfusion and the third term represents the average power dissipated by the RF current, which is:

$$P_d = \frac{\sigma E^2}{2} \tag{4.3}$$

Initially, the cardiac tissue is electrically homogeneous and isotropic. However, as the tissue temperature rises, the local electrical conductivity increases because of electrolytic effects (HAYT, 1981; SCHWAN, 1983). Within the temperature range 25°C-50°C, σ was calculated using:

$$\sigma = \sigma_0 \exp\left(0.02 \times \left(T_k - T_0\right)\right) \tag{4.4}$$

where T is the temperature at any given time and T_0 is the initial temperature (25°C). To simplify programming, the conductivity value obtained from eq.4.4 was used only for the power computations (eq. 4.3) and not for the potential computations (eq. 4.1). As for the thermal conductivity, it was kept constant because of conflicting reports about conductivity increases (VALVANO et al, 1985) or decreases (BHAVARAJU and VALVANO, 1997) with temperature and also because the tissue properties can be altered differently by the rapidity of the temperature rise.

The initial and boundary conditions are: initial temperature of the entire model at 25°C, the room temperature of the *in vitro* studies; the two blood layers at 25°C; continuity of temperature and heat fluxes at the electrode-tissue, insulator-electrode and

insulator-tissue interfaces; and convection at the tissue-blood, electrode-blood and insulator-blood interfaces given by:

$$-k\frac{\partial T}{\partial n}=h(T-T_b) \tag{4.5}$$

where h is the heat transfer coefficient: $h_t = 2000$ W m^{-2} °C^{-1} for the tissue-blood interface; $h_e = 7000$ W m^{-2} °C^{-1} for the electrode-blood interface; $h_i = 7000$ W m^{-2} °C^{-1} for the insulator-blood interface (KAOUK et al., 1996). The values of the electrical and thermal constants for the different regions are presented in Table 4.1. For the valve, we have found only the electrical conductivity $\sigma = 1.3$ S/m, measured by Jang-Zern Tsai (from private communication).

Constant	Unit	blood	tissue	electrode	insulator
Φ	$S*m^{-1}$	0.6	0.3	$9.4*10^6$	0.0
K	$W*m^{-1}*^0C^{-1}$	0.63	0.59	73.0	0.2
ρC	$J*m^{-3}*^0C^{-1}$	$3.7*10^6$	$4.2*10^6$	$2.8*10^6$	$2.4*10^6$

Table 4.1. *Values of electrical and thermal constants.*

The finite-difference method was applied to calculate both the potential distribution and the time-varying temperature distribution using the successive overrelaxation method to accelerate convergence. In preliminary simulations, the implicit method was applied for the temporal computations using time steps ranging from 1 msec

to 100 msec. We found no significant differences in the temperature distributions using the 10-msec time step and the 1 msec time step. Thus, we selected the 10-msec time step for the rest of the simulations. At each time step, the potential was calculated taking into account the electrode movement through the tissue resulting from the application of the "vaporization" rule presented at the beginning of this Section.

4.3.3 Estimation of cellular damage and electroporation

The extent of tissue damage in the vicinity of the catheter was estimated using the Arrhenius equation:

$$\Omega = \int A \times \exp(-E_a / RT)\, dt \tag{4.6}$$

where Ω is the accumulated damage; A, is a frequency factor; E_a, the activation energy (J); R. the universal gas constant ($J * mol^{-1} / K$); T, the temperature ($°K$); t, the time. Values for A and E_a were taken from (LABONTÉ, 1994) $A = 2.39 \times 10^{92} s^{-1}$, $E_a = 5.87 \times 10^5$ $J \times mol^{-1}$. By definition, $\Omega \geq 1$ represents an irreversible damage.

To estimate the extent of the region undergoing electroporation, the maximum transmembrane potential V_m was calculated using the following equation for a cylindrical cell placed in a uniform electrical field with a sinusoidal frequency f and a rms intensity E_{ap}:

$$V_m = \frac{a\, E_{ap}}{\left[1 + (2\pi f \tau_m)^2\right]^{1/2}} \tag{4.7}$$

where a is the half cell length (50 μm) and τ_m is the relaxation time of the membrane (2 msec) (modified by (KINOSITA and TSONG, 1977) from Schwan equation (SCHWAN, 1983)). The electrical field intensity was obtained from the gradient of the potential distribution.

4.4 EXPERIMENTAL PROTOCOL

We performed *in vitro* experiments to investigate the physical mechanisms of RF perforation and to validate the numerical simulations. Hearts were explanted from three mongrel dogs anesthetized with chloralose, small slice of atrial tissue (about 30×30×2 mm) and valves (pulmonary, tricuspid) were dissected and placed in a saline-blood solution at room temperature. RF energy was delivered using a septostomy generator (Baylis Medical Co., Mississauga, Canada) at a frequency of 500 kHz with continuous power output (non pulsed). The voltage and current were automatically adjusted by the generator so as to provide a specified output power (selectable between 1 to 25 W) for a specified duration. The voltage and the load impedance were digitized at 5 samples/sec and the values were stored on a hard disk. A large return electrode was placed at the bottom of the dish containing the tissue.

Two types of active RF electrodes were used: 1) a standard RF perforation catheter (Baylis, 2F size with an electrode length of 1,4 mm); 2) a cylindrical needle having a 0,17 mm radius incorporating a thermocouple (Physitemp) with a short time constant (25 msec). The temperature values were digitized at 20 samples/sec and later

low-pass filtered numerically (10 Hz). However, because of the electrical interference produced by arcing during perforation at high power settings, the temperature measurements were performed only at power settings that were low enough to prevent perforation and arcing. These temperature measurements were compared to the simulated values to validate the numerical model in absence of catheter displacement.

4.5 RESULTS

First, to validate the computed temperatures, the thermocouple needle was inserted about 1 mm inside a myocardial slice in contact with air. The RF power was set at 1 W, a value that was too low to perforate the slice, but high enough to increase the tissue temperature by about 20°C. The average measured voltage was 16 V and the duration of exposure was 7 sec. A numerical simulation was performed using the air-tissue model with the same electrode size, penetration depth, voltage and exposure duration as in the experiment. The temperature of the catheter tip versus time is plotted for both the computed and the measured values in Fig.4.2. These two curves coincide closely during the rising phase, but start to diverge during the cooling phase. The measured temperature is then larger than the simulated temperature, probably because of the heat transfer by air convection at the interface is underestimated. However, because of the excellent agreement between the simulated and measured values during the initial phase, which is critical for the perforation process, the model was considered acceptable.

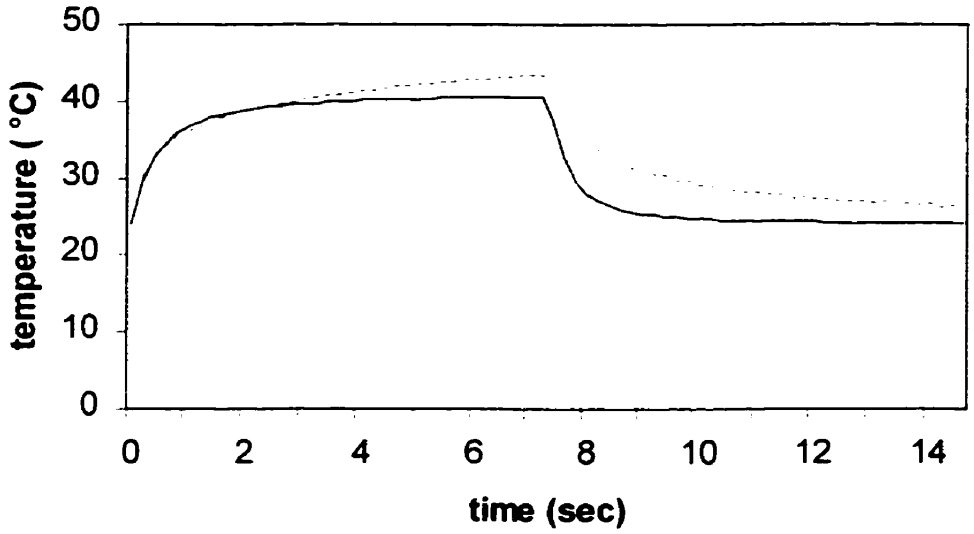

Figure 4.2 *The time courses of the measured (dotted line) and simulated (continuous line) tip temperature during and after energy delivery (1 W). The measured values were obtained from a thermocouple needle inserted in a myocardial slice in contact with air. The numerical simulation was performed using an air-tissue model with the same electrode size, penetration depth, voltage and duration.*

The rapidity of the temperature rise is strongly affected by the applied voltage as can be seen in Fig.4.3, which shows the simulated temperature in the tissue in front of the catheter tip as a function of time for the blood-myocardium-blood model with a static catheter (no perforation). If the voltage is equal or smaller than 70 V, the tissue temperature at the advancing edge stabilizes and does not reach the 100°C, critical point that is necessary for perforation. Also, we note that for the largest potential value, the temperature rise at the onset has a convex shape (non-exponential), reflecting the non

linear effect of the temperature-dependent electrical conductivity. Thus, this simple thermal breakdown model allows us to estimate a critical perforation voltage for a specific electrode geometry, electrode-tissue interface and tissue properties.

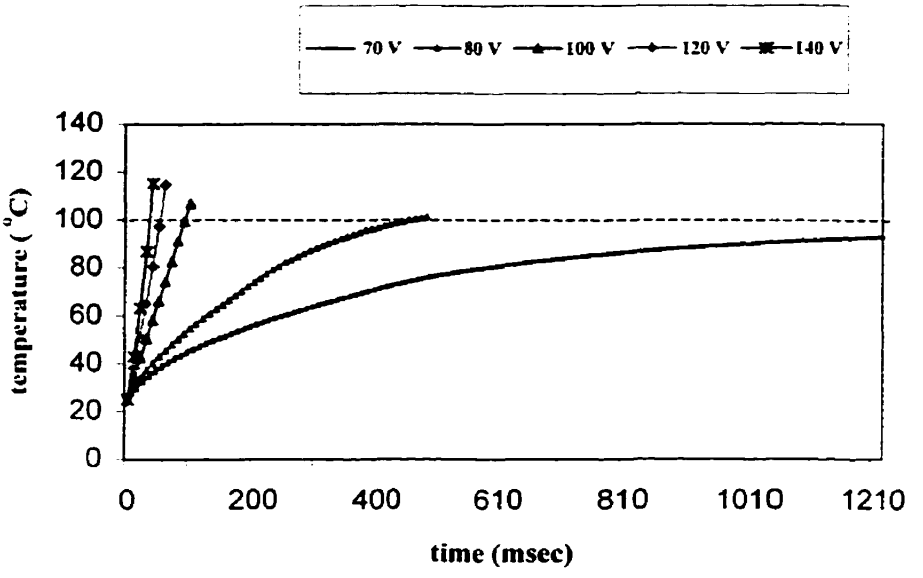

Figure 4.3 *The time courses of the simulated tissue temperature in front of the catheter tip (0.15 mm radius) for different applied voltages using the blood-myocardium-blood model with a static catheter (no perforation)*

Fig.4.4 illustrates the perforation process in the same blood-myocardium-blood model as in the preceding figure using a 120 V electrode potential: the catheter is positioned just over the tissue surface at the immediate onset of perforation (left) and at the end of complete myocardial perforation (300 msec later). Isotherm lines join points

having the same temperature and shading indicates the temperature distribution. We note that the catheter temperature is not uniform and that tissue temperature can greatly exceed 100 °C, mostly on the side of the catheter after perforation. The latter occurs because "tissue vaporization" is programmed only for the points that are immediately in front of the catheter, and not for those on its side. With this model, the perforation speed depends on the applied voltage: the higher the voltage, the higher the speed: 2,2 mm/sec for 80 V; 4,5 mm/sec for 100 V; 7 mm/sec for 120 V.

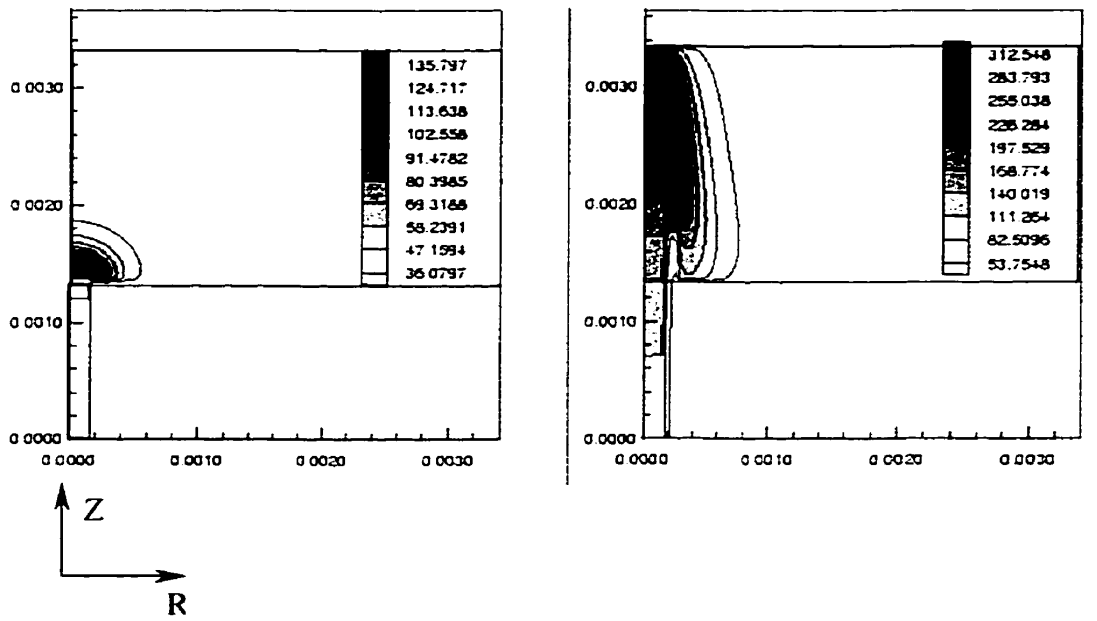

Figure 4.4. *Simulated temperature distributions in the r-z plane at the onset of perforation (left) and after perforation (right, 300 msec later) using the same model as in the preceding figure for a 120 V potential. Isotherm lines join points having the same temperature and shading indicates the temperature distribution.*

The different types of alterations occurring in the tissue can be estimated from the curves showing the tissue temperature (Fig. 4.5, top) and the transmembrane potential (Fig. 4.5, bottom) versus distance in front of the catheter at the onset of perforation for the blood-myocardium-blood model. The extent of the region undergoing estimated desiccation (above 70∘C) is larger, not for a larger applied voltage, but for a smaller voltage because the temperature rises more slowly. In contrast, the extent of the region undergoing estimated electroporation (above 450 mV) is larger for a larger applied voltage because electroporation occurs almost instantaneously. Similarly, the extent of the damaged tissue can be estimated using eq. 4.6 at the onset of perforation (Fig.4.6, left) and after perforation (Fig. 4.6 right). Like desiccation, the extent of the damaged region at perforation onset is larger for a smaller voltage. After perforation, the extent of the damaged region does not differ significantly for the different voltage settings.

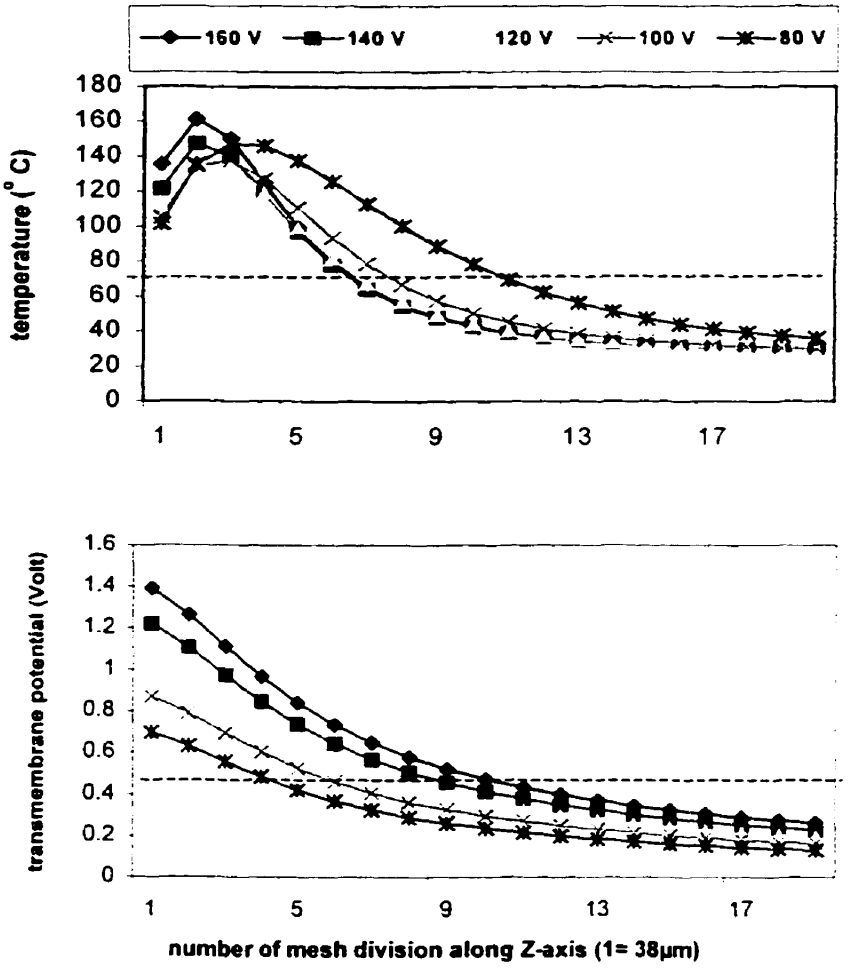

Figure 4.5. *Simulated tissue temperature (top) and transmembrane potential (bottom) versus distance in front of the catheter at the onset of perforation for the same model as in the preceding figure.*

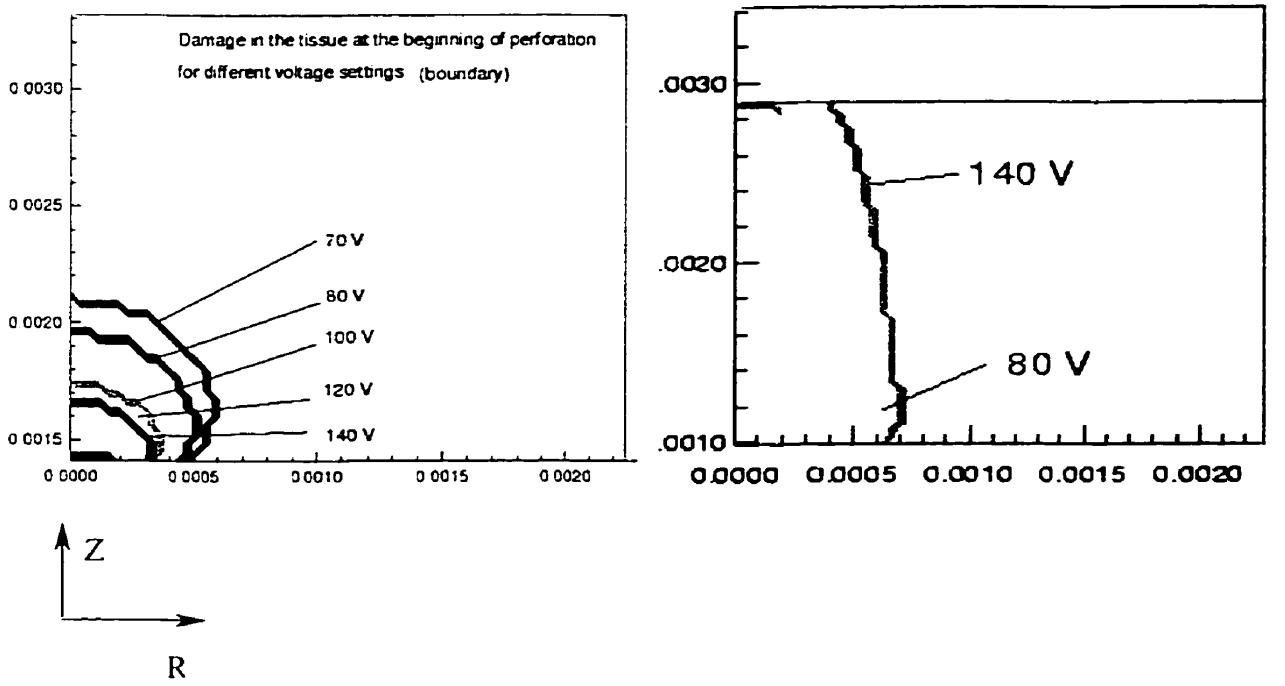

Figure 4.6. *Simulated distribution of damaged tissue (Arrhenius equation) in the r-z plane at the onset of perforation (left) and after perforation (right) for different applied voltages using the same model as in the preceding figure.*

Fig. 4.7 shows the effects of electrode length (top) and radius (bottom) on the time of onset of perforation versus applied voltage for the blood-myocardium-blood model. For the same applied voltage, perforation begins earlier during energy delivery for the shorter electrodes as well as for those with a smaller radius. Also, the electrode with a length of 1 mm can perforate tissue with a minimal voltage setting of 70 V, whereas the critical voltage increases to 80 V for those with a length of 2.0 mm.

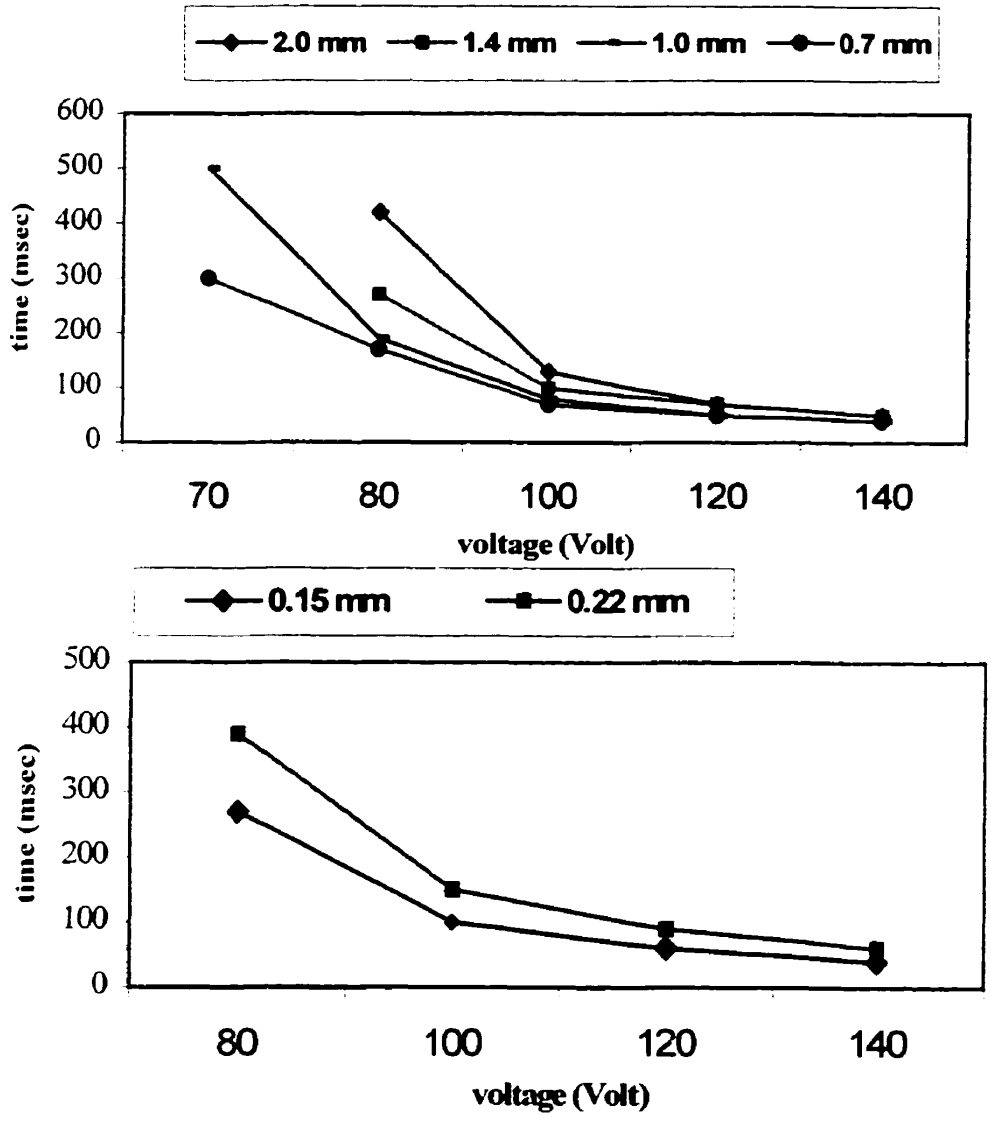

Figure 4.7. *Simulated time of onset of perforation (latency between applied voltage and beginning of perforation) versus voltage for different electrode lengths (top) and electrode radius (bottom) using the same model as in the preceding figure.*

Finally, Fig. 4.8 summarizes the results of 30 RF perforation attempts in atrial myocardium (18 successful and 12 unsuccessful) and 15 RF perforation attempts in valvular tissue (8 successful and 7 unsuccessful) using a 2F catheter with an electrode length of 1,4 mm. The cumulative percentage of successful and unsuccessful attempts is plotted versus applied voltage for myocardial (top) and valvular (bottom) tissue. These experiments were performed *in vitro*. The RF catheter was manually held in contact with the tissue and a slight pressure was applied. The myocardial slices were submerged in the saline-blood mixture. The valves were stretched and exposed to air (because of the ease of manipulation) and a return electrode was clamped to the surrounding tissue. Different attempts were made at different sites over the same tissue. For myocardial tissue, successful perforation could occur with a potential as low as 70 V, and 100% success was achieved at 84 V. For valvular tissue, perforation could occur with a potential as low as 64 V, and 100% success was achieved at 68 V. Histologic analyses of the myocardial tissue showed superficial (about 1-2 cells) damage around the sides of the perforated channel. The lowest rates of perforation for myocardial tissue (about 0.5 mm/sec) were observed at the lowest settings, for which the catheter stuck to the tissue. Any subsequent perforation attempts with the same setting at the same site were unsuccessful.

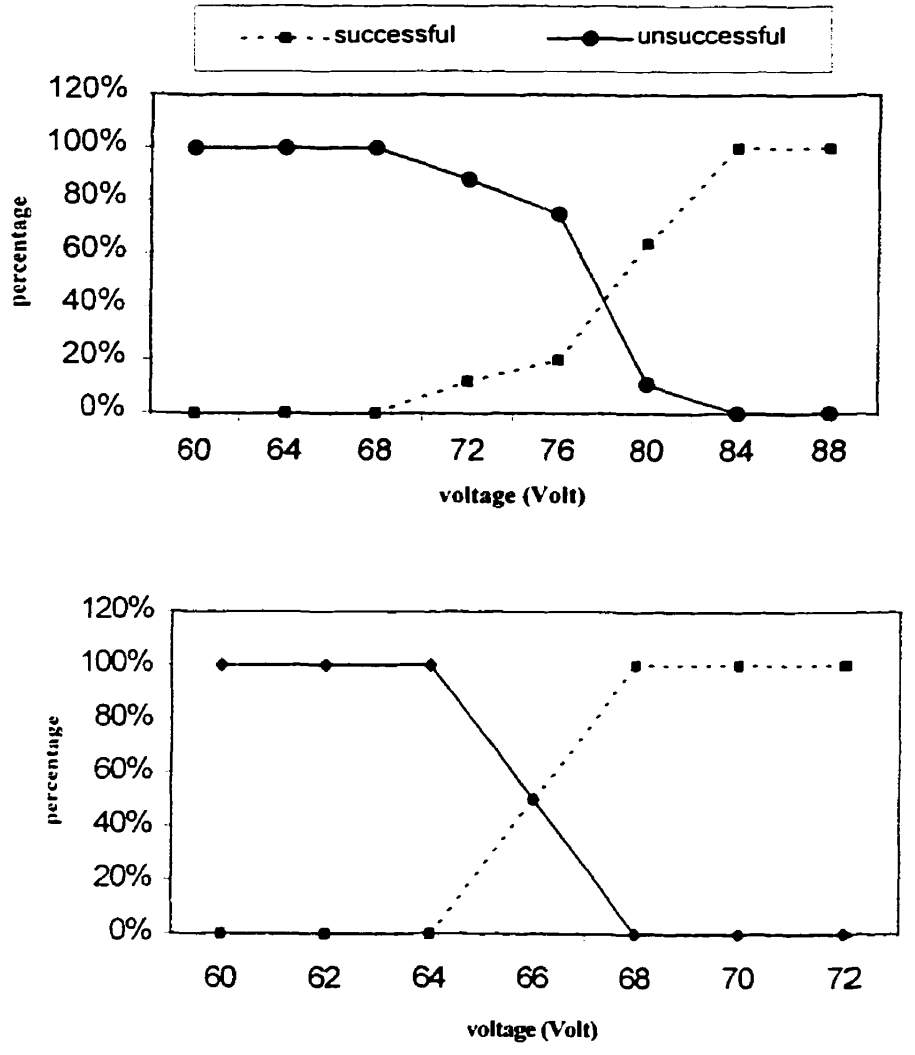

Figure 4.8. *Cumulative distributions of successful (dotted line) and unsuccessful (continuous line) perforation attempts as a function of measured voltage for atrial myocardium in a saline solution (top) and for valvular tissue in air (bottom). The curves represent the percentage of attempts that used voltages below a given value on the horizontal axis.*

The minimum applied power that resulted in myocardial tissue perforation was 13-14 W and the corresponding value calculated with the model was 13,5 W. A small, (3-4 mm) denatured (whitened) region was observed at 13-14 W, the catheter stuck to the tissue and the impedance increased. Less denaturation was observed at a higher power (24 W). The minimum applied power that resulted in valve perforation was 16 W.

The average catheter impedance measured at the onset of energy delivery matched the corresponding value calculated for the myocardium and the valve. A slight impedance decrease was initially observed, reflecting the increase of electrical conductivity with temperature. It was later followed, either by a slight increase in cases of heating without perforation (probably due to coagulum formation), or by drastic increase in cases of perforation (because of electrical arcing).

4.6 Discussion

In contrast with RF catheter ablation used for the treatment of cardiac arrhythmias (Kaouk et al., 1996; Labonté, 1994), RF perforation is a non-linear phenomenon. Perforation occurs only when the applied voltage exceeds a certain threshold that depends on factors such as tissue characteristics, catheter geometry and energy delivery mode. The proposed numerical model, which used a simple 100°C threshold to initiate catheter displacement, was able to reproduce both the tissue temperature rise measured *in vitro* (first phase) and the non-linear behavior associated with perforation (second phase). The

perforation voltage thresholds that were estimated with the model were similar to those observed in isolated myocardial preparations using a catheter with the same geometry.

Design features of the catheter and its RF source permitting predictable perforation with minimal collateral damage to adjacent tissue were identified. The choice of the catheter radius depends on mechanical factors such as the size of the balloon to be inserted through the pulmonary valve and the overall rigidity of the catheter. From an electrical point of view, an increase of the electrode size (length or radius) also increases the voltage threshold for perforation as well as the onset time of perforation for the same voltage setting. As for the collateral damages, increasing the applied voltage or decreasing the electrode length increases the rapidity of the temperature rise and leads to a decrease of collateral damage estimated by the Arrhenius equation. The extent of the region undergoing estimated desiccation is larger, nor for a larger applied voltage, but for a smaller voltage, in contrast, the extent of the region undergoing estimated electroporation increases with the voltage because electroporation occurs almost instantaneously. With lower voltages, desiccation and coagulum formation were also observed experimentally. Desiccation and coagulum can increase the catheter impedance and impair the progression of the catheter through the tissue. Microscopic studies of RF delivery performed by others (PEARSE, 1986; DUFFY and COBB, 1995; HINDRICKS and HAVERKAMP, 1989; AN et al., 1989) have demonstrated discrete areas of desiccated and coagulated tissue for low electrical field intensity, and minimal thermal damage around the perforated site for high electrical field intensity (PEARSE, 1986; DUFFY and COBB, 1995; MELNIK et al., 1994).

Preliminary simulations that compared the effects of continuous versus pulsed current suggest a slight increase in tissue damage and perforation duration when the current was pulsed. With pulsed current, the tissue temperature changes through thermal conduction during the off-phase and the cells undergo a slower rate of heating that may lead to desiccation. Similarly, others have observed extended tissue desiccation with pulsed current waveform (DUFFY and COBB, 1995).

The complex interactions between thermal, electrical and mechanical effects described in Section 4.2 were much simplified in the proposed numerical model. The effects of electroporation, desiccation and protein denaturation on the electrical conductivity and mechanical resistance of the tissue were not specifically incorporated into the model. Neither were the force applied to the catheter, nor the formation and effects of a coagulum. Of all these factors, we feel that electrical arcing is probably the most important since, during all our *in vitro* experiments, no perforation was observed without arcing. This was also observed or suggested by other authors (TUCKER et al., 1992; DUFFY and COBB, 1995).

Electrical arcing reflects the extremely high current density resulting from the dielectric breakdown of polar molecules and the ionization of the steam layer by a high electrical field. Electrical arcing produces rapid changes of catheter impedance (TUCKER et al., 1992; PEARCE, 1988; TUCKER et al., 1984) and may depend on the dielectric strength of the tissue, the current density, the steam layer thickness and pressure, the concentration of residual ions from the previous discharges (PEARCE, 1986), the shape of the electrode, etc. The damage produced by an arc is shallower because of the more

abrupt fall off of the electrical field with distance in the case of a point source (arc) compared to a surface (electrode tip). Ion clouds remaining from previous strikes favor additional strikes along the same pathway and for a continuous a.c. waveform, the arc has a slightly larger cross section and is less intense than the arc formed by a pulsed waveform (TUCKER et al., 1984). A model accounting for the statistical nature of electrical arcing would thus be more complex and time consuming.

Electrical stimulation of the cardiac tissue by the RF current is not possible because of the high frequency of this current (500 kHz). However, tissue excitation may occur because of some degree of rectification induced by the electrical arcing (TUCKER et al., 1984; CURTISS, 1973). Thus, the need to better understand arcing so as to better control it. For example, arcing around hemispherical electrodes is more scattered, uniform and less intense.

4.7 CONCLUSION

A simple numerical model of RF perforation was developed to compute the potential and temperature distributions, and to advance the catheter when a tissue temperature threshold was exceeded. The computed temperature time course coincided with temperature values measured in isolated canine myocardium. Simulated perforation occurred when the applied voltage exceeded 70-80 V in the myocardium, which also coincided with experimental observations. The lateral extent of tissue damage was smaller with a higher voltage because of more rapid perforation. Shorter electrodes with

smaller diameters produced a more rapid perforation. In conclusion, numerical simulations provide insights into such aspects of RF perforation as electrode size, current delivery, speed of perforation and collateral damage.

Project was supported by The National Science Foundation of Canada.

CHAPTER V

ADDITIONAL NUMERICAL AND EXPERIMENTAL RESULTS

In addition to the simulations presented in the previous chapter, the present chapter includes:

- the data on calculated and experimentally measured critical voltages in the myocardial tissue and valve, as well as the simulated temperature rise in the valve;
- the electrical field distribution around the catheter with different electrode tip geometries;
- the electrical parameters measured during our *in-vitro* experiments.

5.1 CRITICAL VOLTAGES: CALCULATED VERSUS EXPERIMENTAL

Table 5.1 summarizes the calculated critical voltages for the thermal breakdown, electroporation, and the experimentally found critical voltage for perforation in myocardium for the next two electrode-tissue arrangements:

- the Baylis catheter placed at right angle to the tissue, a blood layer constitutes the boundary ,
- and the needle thermocouple inserted into the tissue, an air layer constitutes the boundary.

	Baylis catheter	Thermocouple
Calculated critical voltage for thermal breakdown	75V	40 V
Calculated critical voltage for electroporation	65 V	40 V
Experimentally found critical voltage for perforation	75V - 80V	41 V

Table 5.1. *Comparison of the critical voltage for thermal breakdown, the critical voltage for electroporation and the experimentally found critical voltage for perforation in the myocardial tissue.*

Temporal behavior of the numerically calculated temperature in valve at the advancing edge of the electrode for different voltages is shown in Fig.5.1 (numerical model geometry corresponds to our experimental set up for *in-vitro* perforation).

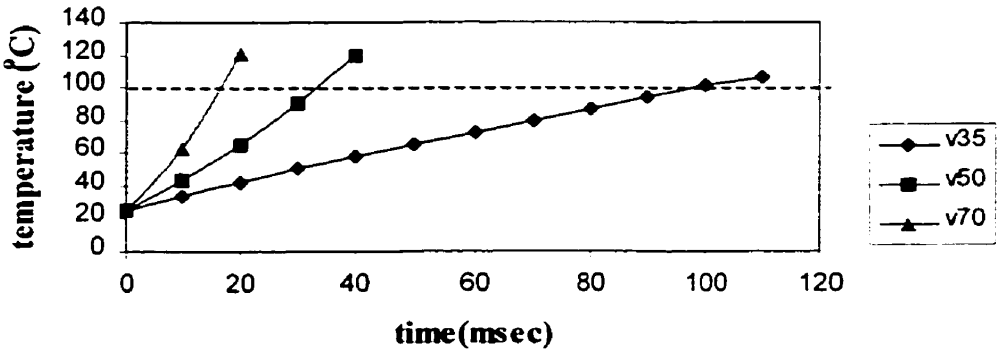

Figure 5.1. *The time courses of the simulated valve temperature in front of the catheter tip (Baylis catheter, 1.4-mm length) for different applied voltages*

If the critical temperature for the valve is 100°C, then the critical voltage corresponding to the thermal breakdown is equal to 35 V. The experimentally derived critical voltage for the valve perforation with the Baylis catheter of the same size is 65 V. We have no data (transmembrane voltage of electroporation) to calculate the critical voltage for electroporation in valve.

5.2 ELECTRICAL FIELD DISTRIBUTION AROUND THE CATHETER WITH DIFFERENT ELECTRODE TIP GEOMERTIES

Numerical simulations allowed to calculate the electrical field distributions around the catheter for different tip geometries as shown in Fig.5.2.

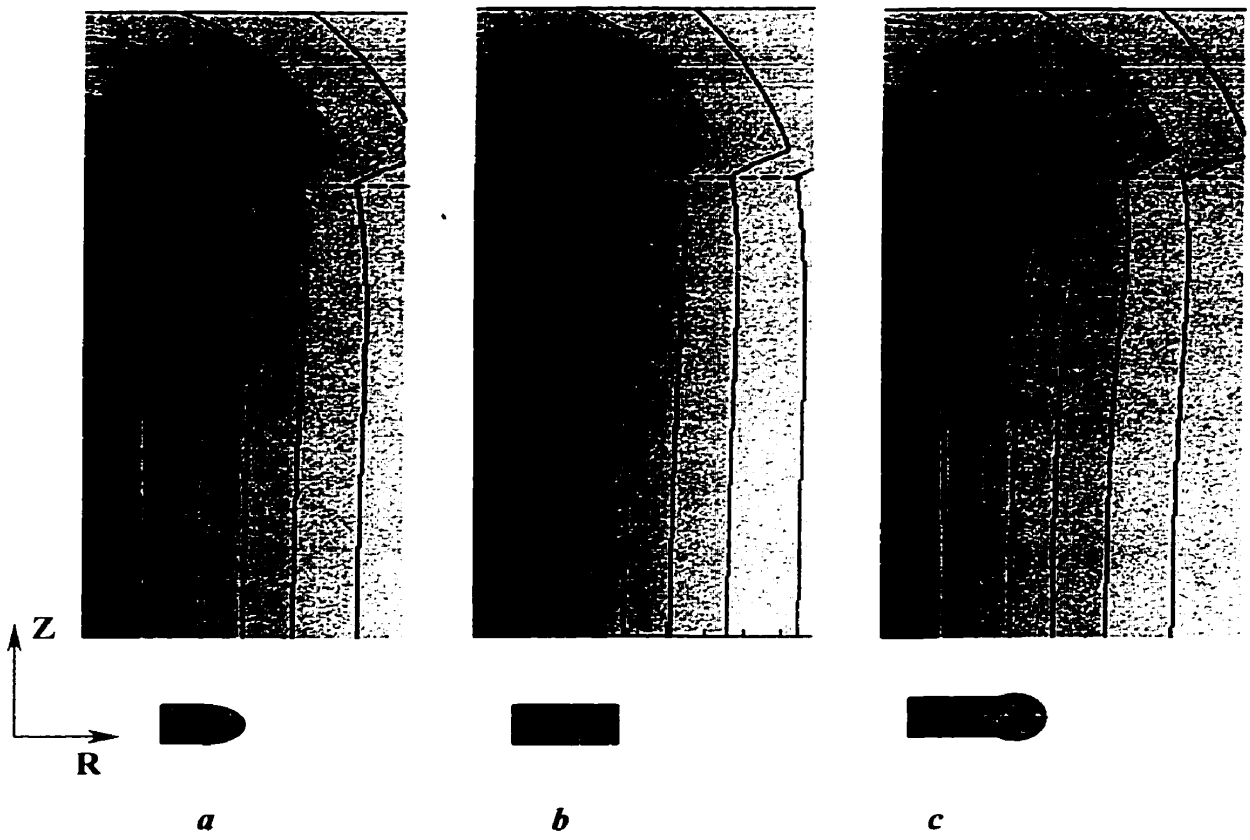

Figure 5.2. *Electrical field distribution (logarithm of electrical field) around the catheter tip for different configurations: a) semispherical, b) cylindrical and c) semispherical with enlargement at the end. Here the horizontal dashed line separates two zones: tissue (upper portion) and blood (lower portion). Maximal values (in front of the catheter tip) are $2.82*10^5$, $2.57*10^5$ and $2.78*10^5$ V/m for a, b, c configurations, correspondingly. The corresponding minimal values are the same for all configurations and equal to 10^4 V/m.*

The electrical field in the tissue (upper portion) is more uniform at the advancing edge of the electrode with the semispherical tip than around the cylindrical tip. However, the electrical field in the blood layer is more pronounced at the side of the enlarged semispherical electrode than at the side of the other electrodes.

A narrow intense arc can occur at the sharp edge of the cylindrical catheter. Hence, the probability of current rectification and tissue stimulation is higher for the catheter with a sharp edge. An excessive heating of the blood layer (as in c) may lead to enhanced blood clot formation. Thus, the optimal geometry of the RF catheter is semispherical (a), i.e. the one with the smallest and uniform curvature radius. An arc formed around such a catheter tip can be scattered over a larger area be more uniform and less intense.

5.3 EXPERIMENTAL DATA: POWER, VOLTAGE, CURRENT AND IMPEDANCE

The following figures show the applied power, voltage, current and impedance as a function of time during myocardial tissue heating without perforation with the Baylis catheter. The Baylis generator was used for current delivery. This generator adjusts the RF voltage so as to maintain a preset power. Change in the electrode-tissue impedance will thus result in current and voltage changes.

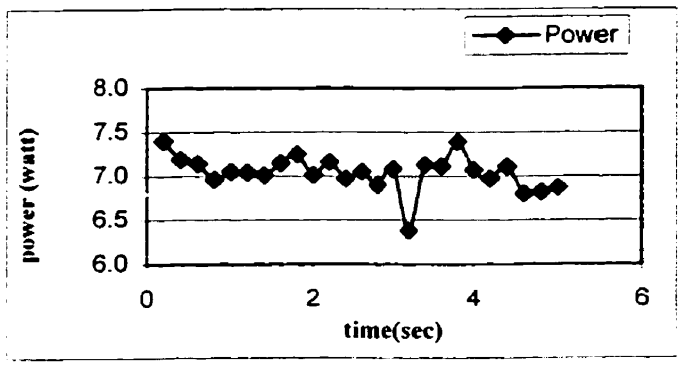

Figure 5.3-1. *Test 40, applied power.*

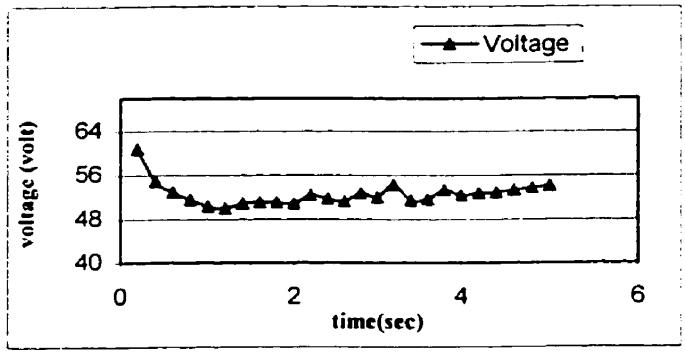

Figure 5.3-2. *Test 40, voltage*

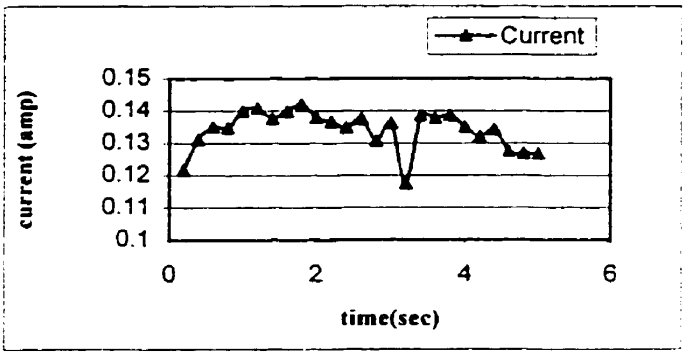

Figure 5.3-3. *Test 40, current*

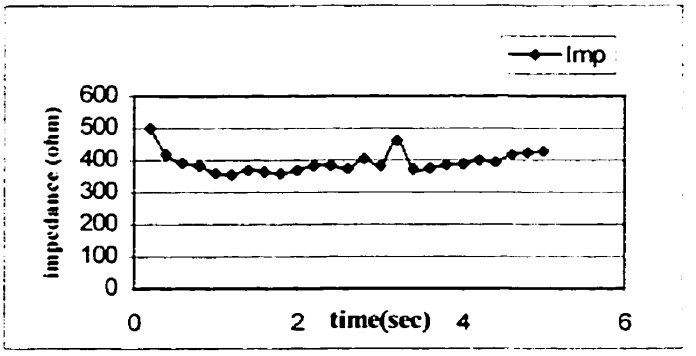

Figure 5.3-4, *Test 40, impedance*

When the voltage is less than 65 V, the current increases and the impedance decreases during the first 3 seconds, reflecting the conductivity increase with temperature. But in the following 2 seconds, the current decreases while the impedance increases. This could be explained by coagulation of the tissue.

With a subsequent power increase, one could observe even larger increase of the impedance (Fig.5.4). In this test a little perforation took place during the last second. But the catheter became stuck to the tissue and was removed applying some force. Recorded voltage attained the critical perforation level. In both cases, a wide area of the tissue around the catheter was whitened.

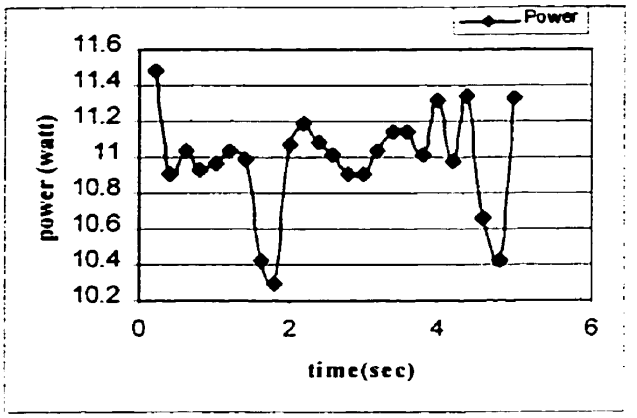

Figure 5.4. *Test 42, power*

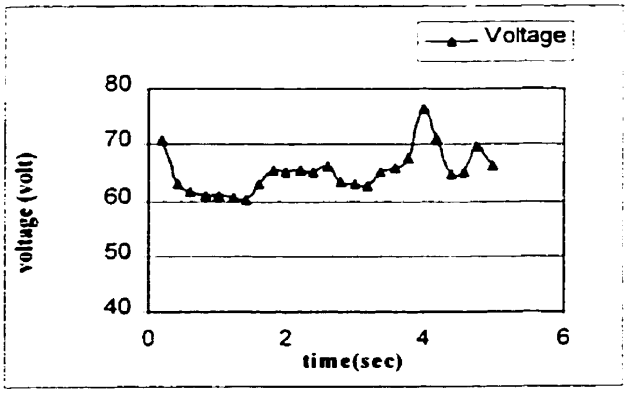

Figure 5.4-2. *Test 42, voltage*

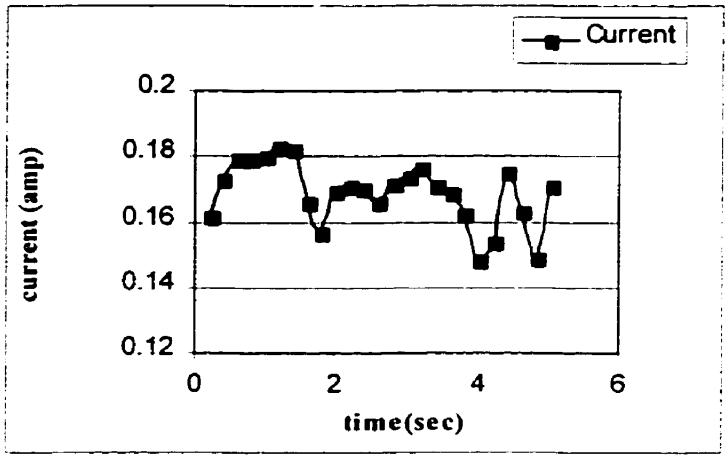

Figure 5.4 – 3. *Test 42, current*

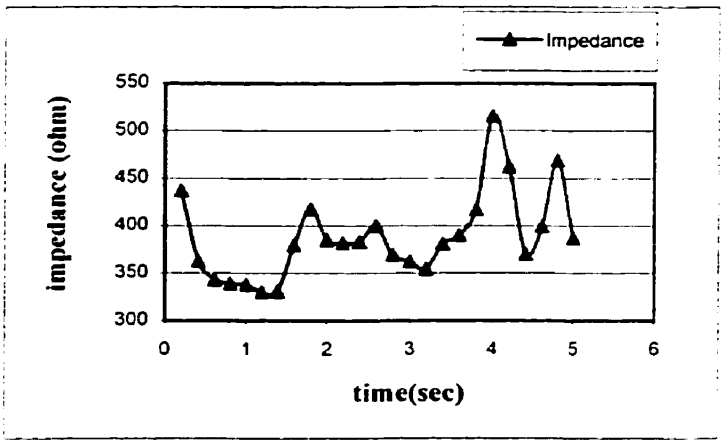

Figure 5.4 – 4. *Test 42, impedance*

If the voltage is above the critical level, perforation takes place. In Fig.5.5 one could observe the abrupt and very large increase of impedance, indicating arcing. The applied power corresponding to the critical voltage of RF perforation in myocardium is about 14 W.

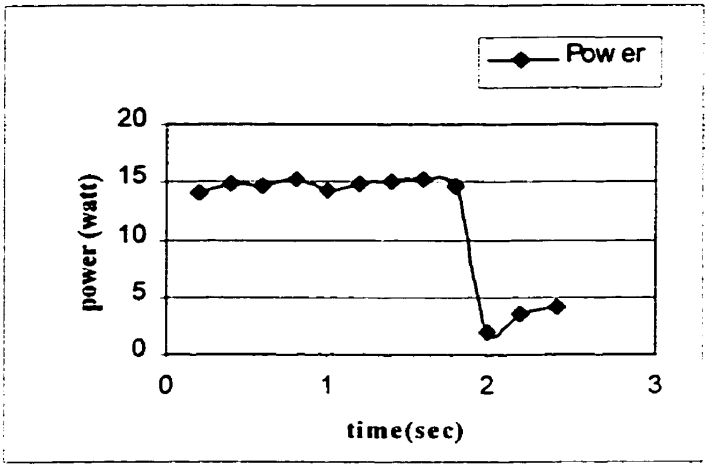

Figure 5.5 –1. *Test 45, power*

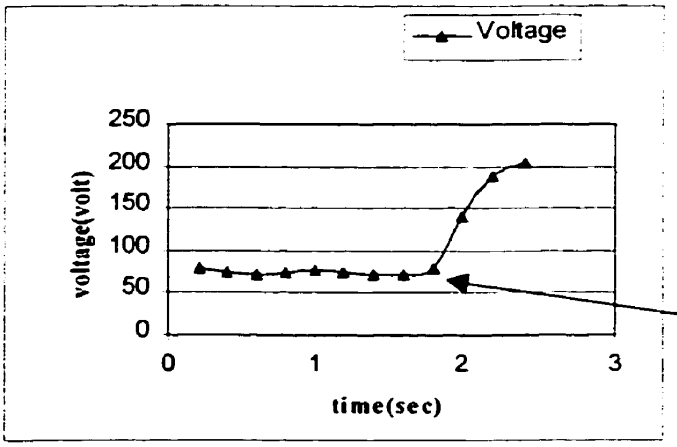

Figure 5.5-2. *Test45, voltage*

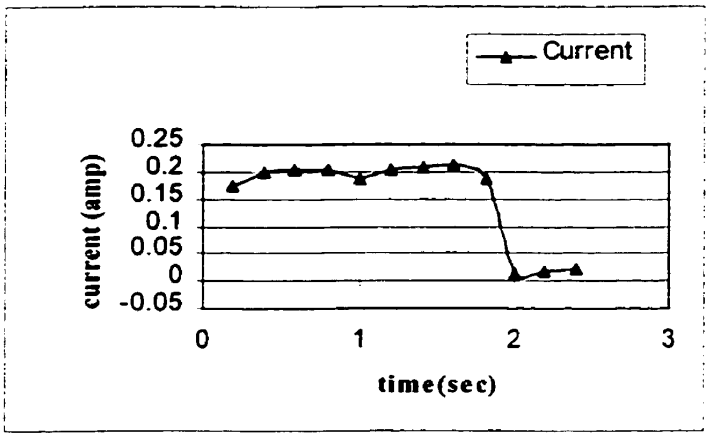

Figure 5.5 – 3. *Test 45, current.*

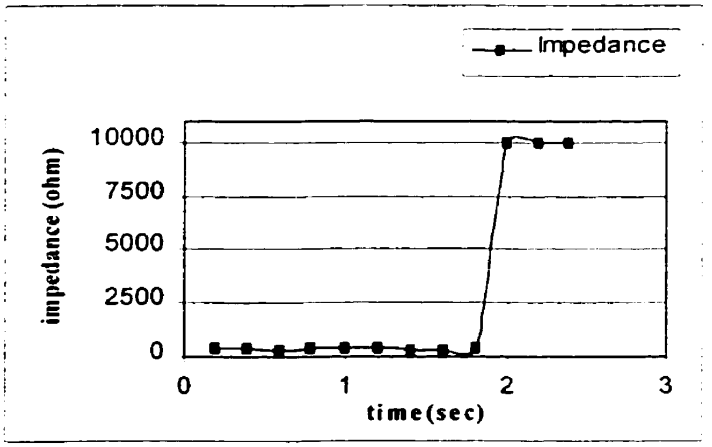

Figure 5.5 –4. *Test45, impedance*

When the initial applied voltage is higher than the critical one, the catheter impedance is smaller. The less extended coagulation or absence of coagulum at the electrode tip in the case of a higher applied voltage could explain this, see Fig.5.6.

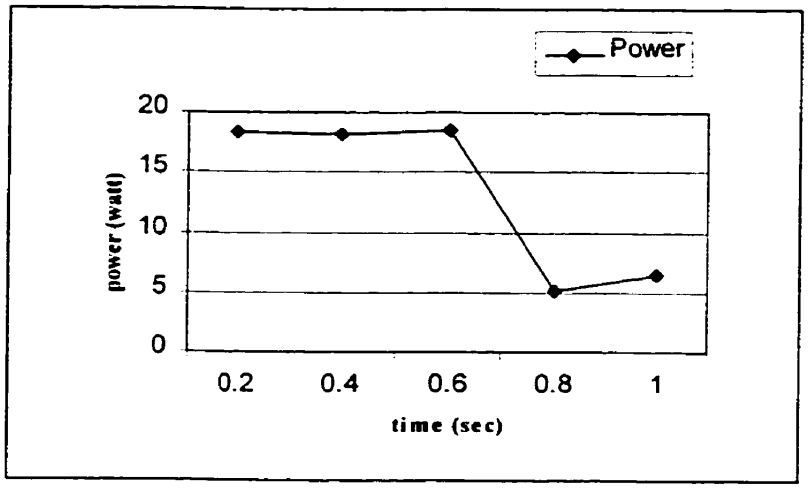

Figure 5.6 – 1. *Test 68, power*

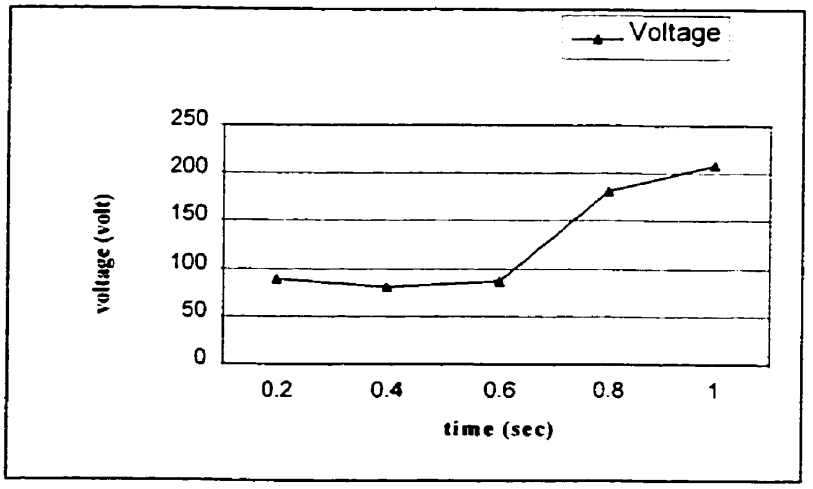

Figure 5.6 – 2. *Test 68, voltage*

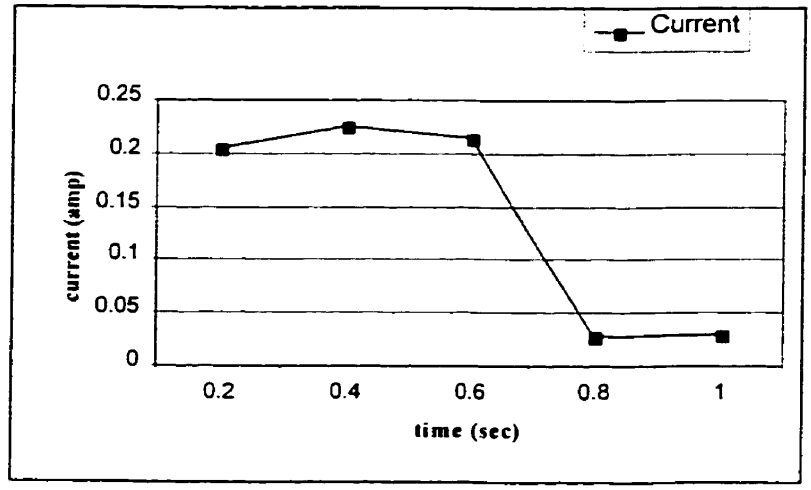

Figure 5.6 – 3. *Test 68, current*

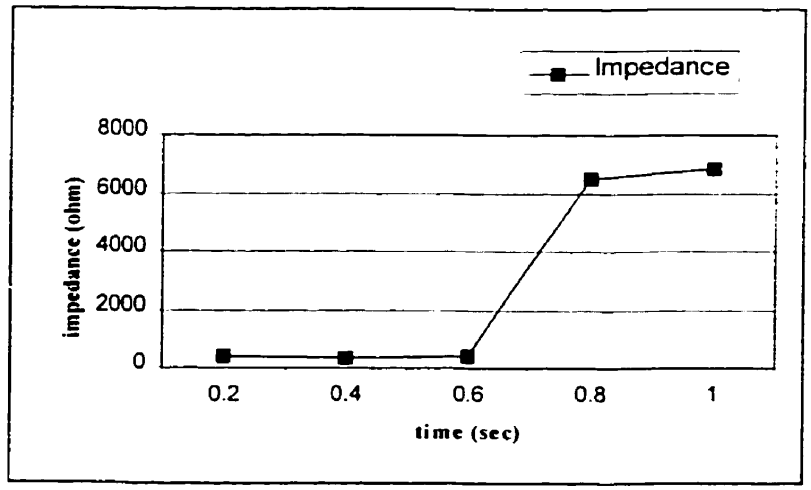

Figure 5.6– 4. *Test 68, impedance*

The smallest area of the whitened tissue around the electrode was observed with the highest delivered power (20-25 W). This corresponds to a voltage of about 100 V. The damaged tissue at the side of the channel is minimal. Only one-cell layer is coagulated. This means that the arcs reduce the damage to the tissue. The initial calculated and experimental catheter impedances are shown in table 5.2.

	Myocardium	Valve
Numerically calculated impedance	420 Ohm	267 Ohm
Experimental impedance	430 Ohm	276 Ohm

Table 5.2. *Numerically calculated and experimentally measured catheter impedances in myocardium and valve.*

CHAPTER VI

DISCUSSION AND CONCLUSION

The present numerical simulation of RF perforation is based on the mechanism of thermal breakdown, which consists of rapid heating of the tissue layer in contact with the electrode up to the water boiling point, subsequent vaporization of a certain amount of the intracellular water and cell explosion. Quantitative description of the myocardial cell electroporation is included into the numerical simulation as well.

The process of the RF perforation is subdivided into two distinct stages: the tissue heating before the onset of perforation and the channel formation.

The first stage includes the tissue heating by known current sources. The close electrode-tissue contact defines the area of current flow. The present mathematical model adequately describes the first stage. The first stage simulations allowed to define the critical voltage of perforation in the myocardium for different electrode tip sizes. The optimal voltage corresponding to the controllable perforation with minimal side effects was identified from the comparison between the temperature distribution in the tissue at the catheter advancing edge and the effect of electroporation at the same site. The optimal voltage corresponds to the perforation with minimal tissue desiccation, minimal possible catheter impedance increase and thus, minimal tissue stimulation. Lateral damage of the tissue at the onset of perforation was also well identified with the numerical simulations.

The assumption of a close electrode-tissue contact for calculating the catheter advance through the tissue (the second stage) allowed applying a deterministic approach to the RF perforation (known current source distribution). The cost of this simplification is an overestimated duration of the RF perforation (twice as fast compared with the experimental duration) and an overestimated lateral tissue damage.

However, the numerical simulation of the second stage of the RF perforation does not correspond to the real process of channel formation, considering numerous arcs in the tissue at the onset of channel formation. The arc formation and the discharge location

depend on many interrelated factors (Chapter 3.3). The RF current transmission from the electrode to the tissue is a random event. This means that the channel formation stage cannot be adequately defined within the present deterministic approach. A more complicated model, based on a statistical approach, could be developed in order to estimate the rate of perforation more accurately. This model will be more time consuming and costly.

Some aspects of arcing were explored within the present study. For example, an optimal catheter tip geometry and optimal voltage were identified in order to minimize both the arc intensity and excitable tissue stimulation.

The valvular RF perforation differs markedly from the myocardial tissue perforation. The numerical simulations of valve perforation based on the thermal breakdown mechanism failed to identify the critical voltage of valve perforation. The experimentally found critical voltage for the valve perforation with the Baylis catheter was 65 V, and the numerically calculated one was 35 V, while the calculated and experimental catheter impedances coincided better. One might assume that the critical voltage of electroporation in valve is much higher than the thermal critical voltage. To be able to calculate the critical voltage of electroporation in valve, the knowledge of the critical transmembrane voltage of electroporation in valve, as well as the size of the valve unit structure is required.

Further numerical simulations of the RF perforation might:

- simulate the valve perforation with all required data for electroporation;
- perform numerical simulation using a coaxial catheter (bipolar) with different radii;
- incorporate the mechanism of electroporation and arcing.

REFERENCES

AN, H., SAKSENA, S., JANSSEN, M., OSYPKA, P. (1989): 'Radiofrequency ablation of ventricular myocardium using active fixation and passive contact catheter delivery systems', American *Heart Journal*, **118**, pp.69-77

BARLOW, D. E. (1982): 'Endoscopic applications of electrosurgery. Review of basic principles', Gastrointestinal *Endoscopy*, **28**, pp.73-76

BENZ, R., BECKER., F., ZIMMERMANN, U. (1979): 'Reversible electrical breakdown of lipid bilayer membranes: a charge-pulse relaxation study', *Journ. Membrane Biol.*, **48**, pp.181-204

BENZ, R., ZIMMERMANN, U. (1981): 'The resealing process of lipid bilayer after reversible electric breakdown', *Bioch.Biophys.Acta*, **640**, pp.169-178

BHAVARAJU, N.C., VALVANO, J.W. (1997): 'Thermal conductivity and diffusivity in swine myocardium', Proc.-19-th Int.Conf. IEEE/EMBS, Oct.-Nov. Chicago,Il.USA

CHANG, D.C., REESE, T.S. (1990): 'Changes in membrane structure induced by electroporation as revealed by rapid freezing electron', *Biophys.Journ.*, **58**, pp.1-12

COSTER, H.G., ZIMMERMANN, U. (1975): ' The mechanism of electrical breakdown in the membrane of vanonai utricularis', *Journ. of Membrane Biology*, **22(1)**, pp.73-79

CURTISS, L.E. (1973): 'High frequency current in endoscopy: a review of principles and precautions', *Gastrointestinal Endosc.*, **20**, pp.9-12

DUFFY, S., COBB, G.V. (1995): 'Practical Electrosurgery', Chapman and Hall Medical, London, pp.15-61.

FONTES, V.F., ESTEVES, C.A., BRAGA, S.L., ACUNA, U., SANTANA, M.V., De OLIVEIRA, L.M., PEDRA, S.R., SOUSA, J.E. (1995): 'Pulmonary atresia with intact ventricular septum. Valvar perforation by radiofrequency', [Portuguese], *Arquivos Brasileiros de Cardiologia* , **64**(3), pp.231-233

GIUSTI, S., SPADONI, I., De SIMONE, L., CARMINATI, M. (1996): 'Radiofrequency perforation in pulmonary valve atresia and intact ventricular septum', [Italian], *Giornale Italiano di Cardiologia*, **26**(4), pp.391-397

HAUSDORF, G., SCHNEIDER, M. (1993): 'Interventional high frequency perforation and enlargement of the outflow tract of pulmonary atresia', [German], *Zeitschrift fur Kardiologie*, **82**(2), pp.123-130

HAUSDORF, G., SCHULZE-NEICK, I., LANGE, P.E. (1993): 'Radiofrequency-assisted "reconstruction" of the right ventricular outflow tract in muscular pulmonary atresia with ventricular septal defect', *British Heart Journal*, **69** (4), pp.343-346

HAYT, W. (1981): 'Engineering Electromagnetics', 4-th ed. Mc.Graw-Hill, New-York

HINDRICKS, G., HAVERKAMP, W. et al. (1989): 'Radiofrequency coagulation of ventricular myocardium: Improved prediction of lesion size by monitoring catheter tip temperature', *European Heart Journal*, **10**, pp.972-984

HOFBECK, M., WILD, F., SINGER, H. (1994): 'Interventional treatment of pulmonary atresia with intact ventricular septum by high frequency perforation and balloon dilatation of the pulmonary valve', [German], *Klinische Pediatrie*, **206**(3), pp.157-160

HONIG, W.M. (1975): 'The mechanism of cutting in electrosurgery', *IEEE Trans.Biomed.Eng.*, **22**, pp.58-62

KAOUK, Z., VAHID SHAHIDI, A., SAVARD, P., and MOLIN, F. (1996): 'Modeling of myocardial temperature distribution during radio-frequency ablation', *Med.&Biolog.Eng.&Comp. Communication*, **34**, pp.165-170

KIM, P.S., BALDWIN, R.L. (1982): 'Specific intermediates in the folding reaction of small proteins and the mechanisms of protein folding', *Annual Rev.Biochem.*, **51**, pp.459-489

KINOSITA, K., TSONG, T. (1977): 'Voltage induced pore formation and hemolysis of human erythrocytes', *Biochimica et Biophysica Acta*, 471, pp.227-242

KNISLEY, S.B. (1994): 'Transmembrane potential at the end of ventricular myocytes during electroporation by field stimulation (abstract)', PACE, **17**, p.838

KRASSOWSKA, W. (1995): 'Effect of electroporation of transmembrane potential induced by defibrillation shocks', *PACE*, **18**(p.1), pp.1644-1659

LABONTÉ, S. (1994): 'Numerical model for radio-frequency ablation of the endocardium and its experimental validation', *IEEE Trans. Biomed.Ing.*, **41**, n2, pp.108-115

LOPEZ, A., ROLS, M.P., TEISSLE, J. (1988): ' P.NMR analysis of membrane phospholipid organization in viable', *Biochemistry,* **27**, pp.1222-1228

MELNIK, I., DUPOUY, P., KVASNICKA, J., BRATIA, A., GESCHWIND, H.J. (1994): 'In vitro study of a radiofrequency guidewire aimed at recanalization of totally occluded peripheral arteries', *Catheterization and Cardiovascular Diagnosis*, **33**, pp. 189-196

PEARCE, J.A. (1986): 'Electrosurgery'. Chapman and Hall, London. pp.62-129

PEARCE, J.A. (1988): 'Electrosurgery'. In Handbook of Biomedical Engineering. Acad.press Inc. pp. 99-121

PERLOFF, J.K. (1987): 'The clinical recognition of congenital heart disease', Saunders Company, Philadelphia, pp.540-551

SALE, A.J., HAMILTON, W.A. (1967): 'Effect of high electric field on microorganism', *Biochim.Biophys.Acta*, **148**, pp.781-788

SCHNEIDER, M., SCHRANZ, D., MICHEL-BEHNKE, I., OELERT, H. (1995): 'Transcatheter radiofrequency perforation and stent implantation for palliation of pulmonary atresia in a 3060g infant', *Catheterization and Cardiovascular Diagnosis*, **34**, pp.42-45

SCHWAN, H.P. (1983) 'Biophysics of diathermy', Chapter III: Therapeutic Heat and Cold, Waverly Press, Baltimore

SCHWAN, H.P. (1983): 'Biophysics of interaction of electromagnetic energy with cells and membranes'. In Biological effects and dosimetry of nonionizing radiation. Ed. by Grandolfo M. and Michaelson S.M. and Rindi A., Plenum Rose, New York, pp.213-231

SONG, L., AHKONG, Q., BALDWIN, J., O'REILLY, R., LUCY, J. (1993): 'Divalent cations, phospholipid asymmetry and osmotic swelling in electrically-induced lysis', *Biochim.Bioph.Acta*, **1148**, pp.30-38

TESSSIE, J., TSONG, T.Y. (1981): 'Electric field-induced transient pores in phospholipid bilayer vesicles', *Biochemistry*, **20**, pp.1548-1554

TOVAR, O., TUNG, L. (1991): 'Electroporation of cardiac cell membrane with monophasic or biphasic rectangular pulses', *PACE*, **14**, pp. 1887-1892

TSONG, T.Y. (1991): 'Electroporation of cell membranes', *Biophys.J.*, **60**, pp.297-306

TUCKER, R.D., SCHMITT, O.H., SIEVERT, C.E., SILVIS, S.E. (1984): 'Demodulated low frequency current from electrosurgical procedures', *Surgery,Gynecology and Obstetrics*, **159**, pp.39-43

TUCKET, R.D., SIEVERT, C.E., KRAMOLOWSKY, E.V., SILVIS, S.E. (1992): 'The interaction between electrosurgical generators, endoscopic electrodes and tissue', *Gastrointestinal Endoscopy*, **38**, pp.118

VALVANO, J.M., COCHRAN, J.R. and DILLER, K.R. (1985): 'Thermal conductivity and diffusivity of biomaterials measured with self-heated thermistors', *Int.J.Thermophys.*, **6**, pp.301-311

WEAVER, J.C. (1993): 'Electroporation: a general phenomenon for manipulating cells and tissues', *Jour. of Cell. Biochemistry*, **51**, pp.426-435

WHITE, S.H. (1974): 'Comments on electrical breakdown of bimolecular lipid membrane', *Biophys.J.*, **14**, pp.15-158

ZIMMERMAN, U. (1982), 'Electric field-mediated fusion and related electrical phenomena', *Biochim.Biophys.Acta*, **694,** pp.227-277

APPENDIX

ELECTRICAL FIELDS IN ELECTROSURGERY

The force acting on a charge at rest or in motion is expressed by the Faraday formula:

$$\vec{F} = q\vec{E} + q\vec{v} \times \vec{B} \qquad \text{(A.1)}$$

where: $\vec{F}$ is the vector force (N) on a charge, q is the charge in coulomb (C), $\vec{E}$ is the electric field intensity around q *(V/m)*, $\vec{v}$ is the velocity of the charge (*m/sec*), $\vec{B}$ is the magnetic flux density around q (T).

There are two general classes of charges: free charges (ions in solution) and bounded charges (molecules of a crystal structure in a dielectric medium). Bounded charges are constrained to either rotational or vibrational motion in response to electric field, while free charges are able to move translationally as well as rotationally and vibrationally. In true electrostatic problem, the charge is restricted from moving in response to the field either being placed on a conducting surface or being bound to the crystal structure of a dielectric medium. In the quasi-static case, free charges are allowed to move through any conductive medium in addition to residing on the surface of conductors, ignoring any magnetic field effects. Thus the equation (A.1) in the quasi-static case takes the form:

$$\vec{F} = q\vec{E} \qquad \text{(A.2)}$$

A free charged particle will be accelerated by a local electric field, moving in the direction either parallel or anti-parallel to the field depending the sign of the charge.

For the RF range in electrosurgery (500 kHz to 3 MHz) the biological medium can be regarded as purely resistive. The magnetic field is of negligible strength, the wavelength is long compared to the size of the object under study (tissue layer in the

vicinity of the electrode). It can be reasonably assumed that the field has the same phase over the tissue layer. Thus in electrosurgery, the quasi-static assumption holds well.

A.1. OHM'S LAW

When an electric field is applied on a free charge distribution, the particles accelerate until their characteristic (for the given medium) drift velocity is reached. Drift velocity depends on the mobility of the charge, which is physically related to its mean free path and other quantum collision statistics. Mobility of the charge depends on temperature as well. The moving charges establish a sort of flux density (C/sec/m^2) or current density (A/m^2). The relation between the current density and the electrical field is generally expressed as:

$$\begin{bmatrix} J_x \\ J_y \\ J_z \end{bmatrix} = \begin{pmatrix} \sigma_{xx} & \sigma_{xy} & \sigma_{xz} \\ \sigma_{yx} & \sigma_{yy} & \sigma_{yz} \\ \sigma_{zx} & \sigma_{zy} & \sigma_{zz} \end{pmatrix} * \begin{bmatrix} E_x \\ E_y \\ E_z \end{bmatrix} \tag{A.3}$$

In the quasi-static case, the off-diagonal terms in the conductivity matrix are zeros. In inhomogeneous materials the conductivity is a function of position, due to the structured nature of the tissue. However, it is possible to estimate the field quantities by enforcing the assumption of homogeneity for the regions of similar tissue type. The solution of the field equation is then separable into regional fields with appropriate boundary conditions at the interfaces. The current density in a finite, homogeneous region is related to the electric field:

$$\begin{bmatrix} J_x \\ J_y \\ J_z \end{bmatrix} = \begin{pmatrix} \sigma_{xx} & 0 & 0 \\ 0 & \sigma_{yy} & 0 \\ 0 & 0 & \sigma_{zz} \end{pmatrix} * \begin{bmatrix} E_x \\ E_y \\ E_z \end{bmatrix} \tag{A.4}$$

Also for the RF current, it is appropriate to assume that the tissue is isotropic (the properties do not depend on the direction). Thus the relation between the current density and the electric field reduces to

$$\vec{J} = \sigma \vec{E} \tag{A.5}$$

and:

$$\sigma = \mu n q , \tag{A.6}$$

where σ is the electrical conductivity (S/m), μ is the mobility of charge carriers in the medium ($m^2/V/sec$), n is the charge carrier concentration (number/m^3), q is the charge of each carrier (C).

The electrical conductivity in biological medium is a function of temperature:

$$\sigma(T) = \sigma_o \, exp[0.02 * (T - T_0)] , \tag{A.7}$$

where $\sigma(T)$ is the electrical conductivity at temperature T (S/m), σ_0 is the conductivity at temperature T_0.

Under the quasi-statistical assumption, the electrical potential in the tissue satisfies the Laplace equation:

$$\nabla (\sigma \nabla V) = 0 \tag{A.8}$$